CASL-ISAND2017-12874R

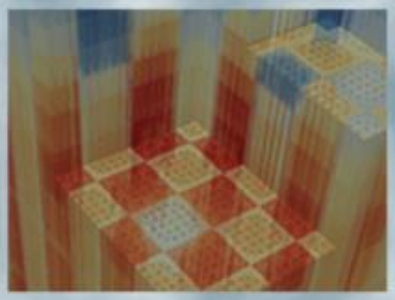

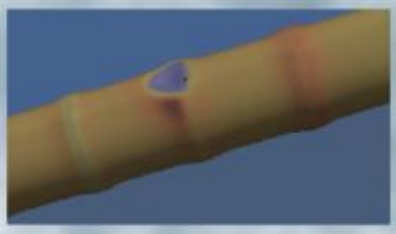

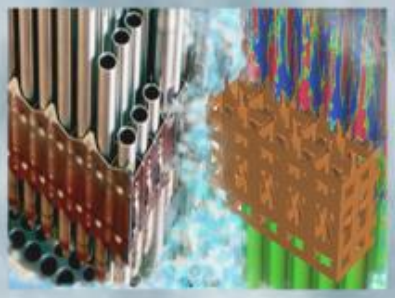

CTF (Subchannel) Calculations and Validation L3:VVI.H2L.P15.01

Natalie Gordon, Sandia National Laboratories

September 5, 2017

Sandia National Laboratories is a multimission laboratory managed and operated by National Technology and Engineering Solutions of Sandia, LLC, a wholly owned subsidiary of Honeywell International, Inc., for the U.S. Department of Energy's National Nuclear Security Administration under contract DE-NA0003525.

Sandia National Laboratories

U.S. DEPARTMENT OF ENERGY | Nuclear Energy

REVISION LOG

Revision	Date	Affected Pages	Revision Description
0		All	Initial Release

Document pages that are:

Export Controlled _____

IP/Proprietary/NDA Controlled_____

Sensitive Controlled_____

Requested Distribution:

To:

Copy:

CONTENTS

FIGURES

TABLES

ACRONYMS

AMA	Advanced Modeling Applications
CASL	Consortium for Advanced Simulation of Light Water Reactors
CHF	Critical Heat Flux
CIPS	CRUD-induced power shift
CFD	computational fluid dynamics
CP	Challenge Problem
CTF	COBRA-TF subchannel thermal-hydraulics code
DNB	departure from nucleate boiling
DOE	US Department of Energy
FA	Focus Area
Hi2Lo	High to Low
LANL	Los Alamos National Laboratory
LWR	light water reactor
M&S	modeling and simulation
NCSU	North Carolina State University
ORNL	Oak Ridge National Laboratory
PWR	pressurized water reactor
QOI	quantity of interest
R&D	research and development
SA	sensitivity analysis
SNL	Sandia National Laboratories
T/H	thermal-hydraulics
UQ	uncertainty quantification
V&V	verification and validation
VVI	Verification and Validation Implementation
VUQ	Validation and Uncertainty Quantification
VVUQ	Verification, Validation and Uncertainty Quantification
WEC	Westinghouse Electric Company

1. INTRODUCTION

The goal of the Verification and Validation Implementation (VVI) High to Low (Hi2Lo) process is utilizing a validated model in a high resolution code to generate synthetic data for improvement of the same model in a lower resolution code. This process is useful in circumstances where experimental data does not exist or it is not sufficient in quantity or resolution. Data from the high-fidelity code is treated as calibration data (with appropriate uncertainties and error bounds) which can be used to train parameters that affect solution accuracy in the lower-fidelity code model, thereby reducing uncertainty.

This milestone presents a demonstration of the Hi2Lo process derived in the VVI focus area. The majority of the work performed herein describes the steps of the low-fidelity code used in the process with references to the work detailed in the companion high-fidelity code milestone (Reference 1). The CASL low-fidelity code used to perform this work was Cobra Thermal Fluid (CTF) and the high-fidelity code was STAR-CCM+ (STAR). The master branch version of CTF (pulled May 5, 2017 – Reference 2) was utilized for all CTF analyses performed as part of this milestone. The statistical and VVUQ components of the Hi2Lo framework were performed using Dakota version 6.6 (release date May 15, 2017 – Reference 3). Experimental data from Westinghouse Electric Company (WEC – Reference 4) was used throughout the demonstrated process to compare with the high-fidelity STAR results.

A CTF parameter called Beta was chosen as the calibration parameter for this work. By default, Beta is defined as a constant mixing coefficient in CTF and is essentially a tuning parameter for mixing between subchannels. Since CTF does not have turbulence models like STAR, Beta is the parameter that performs the most similar function to the turbulence models in STAR. The purpose of the work performed in this milestone is to tune Beta to an optimal value that brings the CTF results closer to those measured in the WEC experiments.

1.1 Milestone Tasks

This milestone, L3:VVI.H2L.P15.01, and the companion milestone, L3:VVI.H2L.P15.02, began with a few introductory steps before splitting into individual tasks. These steps included checking conservation equations and crossflow magnitude in each of the codes. Checking these introductory steps ensures that the simulations are set up the same before calibration is performed.

The workflow is provided in Figure 1. The majority of this report will focus on the CTF Steps with reference to the Initial Steps and the STAR Steps. The CTF steps labeled “0” are introductory steps that laid the ground work for the Hi2Lo process. The experimental data that was provided by WEC was divided into two groups, validation and calibration. Fluid properties from CTF were printed to output and used to construct input fluid property polynomials for STAR. This was another method of ensuring that CTF and STAR were as similar as possible before calibration.

The Hi2Lo process began with validation to determine how far the CTF results were from the experimental results. Bayesian calibration was then performed followed by another validation step to determine the improvement due to calibration. An Experimental Design process was performed to obtain further insight as to the optimal value for the calibration parameter. The final step covered in this report is a final validation step to determine the improvement due to the Experimental Design step. Step 7 in Figure 1 is future work.

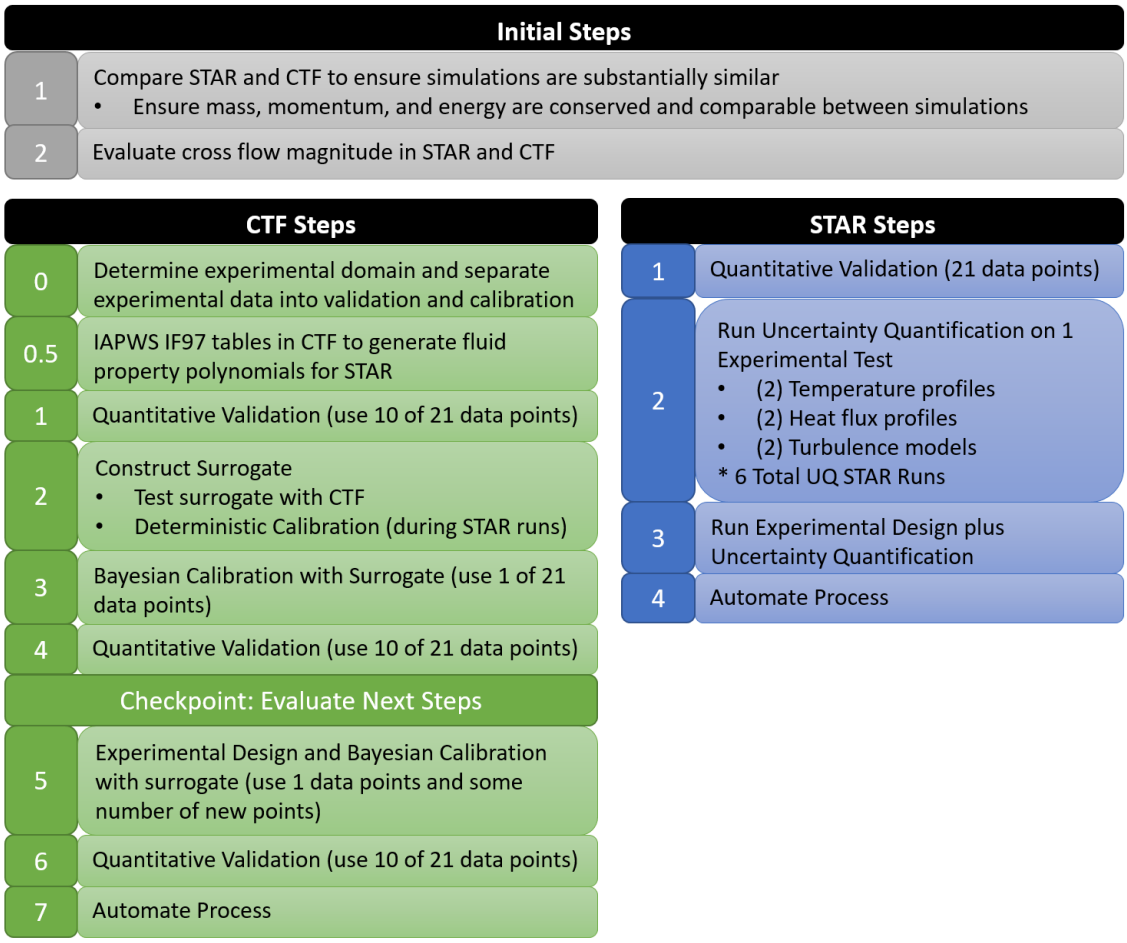

Figure 1. Milestone tasks and workflow for the full Hi2Lo process.

1.2 Working Group and Acknowledgements

The working group for this milestone included Natalie Gordon (SNL), Lindsay Gilkey (SNL), Ralph Smith (NCSU), Brian Williams (LANL), Vince Mousseau (SNL), Chris Jones (SNL), and Adam Hetzler (SNL). Experimental data expertise was solicited from Yixing Sung and Emre Tatli of WEC and Dakota technical support was provided by Brian Adams (SNL), Laura Swiler (SNL), Adam Stephens (SNL), and Kathryn Maupin (SNL).

A technical review was performed by Ralph Smith, Brian Williams, Vince Mousseau, and Adam Hetzler.

2. INITIAL STEPS

Before commencing the high to low (Hi2Lo) process, two initial steps were performed to verify that CTF and STAR boundary conditions were set appropriately so that the chosen parameter is calibrated based on physics, not unintended input differences. The first step was to compare mass, energy, and momentum conservation between codes. The second step was to compare crossflow magnitude.

2.1 Compare Conservation in CTF and STAR

The three conservation quantities of interest were mass, energy, and momentum. A summary comparison of the calculated values is provided in Table 1 and full derivations of the conservation equations are given in Reference 1.

Mass conservation was evaluated according to the following expression:

$$\left(\sum_{i=1}^{36} \rho_i u_i A_i\right)_{outlet} = \left(\sum_{i=1}^{36} \rho_i u_i A_i\right)_{inlet}$$

Where i is the subchannel number, 36 is the total number of subchannels, ρ_i is the density per subchannel, u_i is the velocity per subchannel, and A_i is the subchannel area. The quantity of interest in comparison between CTF and STAR was mass flow rate. The inlet mass flow rate remained constant from inlet to outlet of each code and was the same to three significant figures between codes.

Conservation of energy was calculated using the expression:

$$\left(\sum_{i=1}^{36} \rho_i u_i A_i \left(h_i - \frac{P_i}{\rho_i}\right)\right)_{inlet} + \dot{Q}_{in} = \left(\sum_{i=1}^{36} \rho_i u_i A_i \left(h_i - \frac{P_i}{\rho_i}\right)\right)_{outlet}$$

where P_i is power per subchannel, h_i is specific enthalpy, and $\dot{Q}_{in}$ is the power applied to the heated rods. Power in MW was the same between the inlet and outlet of each code as well as the same value for both codes.

Conservation of momentum cannot be directly compared between codes since CTF and STAR calculate momentum differently. CTF uses the following expression for momentum:

$$\frac{\partial \rho u}{\partial t} + \frac{\partial \rho u^2}{\partial x} = -\frac{\partial P}{\partial x} - Fu^2 - Hu^2$$

where F is the friction factor and H represents the loss coefficients defined in the CTF input deck. STAR uses the compressible Navier-Stokes equation, shown here in 1-D for comparison:

$$\frac{\partial \rho u}{\partial t} + \frac{\partial \rho u^2}{\partial x} = -\frac{\partial P}{\partial x} + \mu \frac{\partial^2 u}{\partial x^2} + \rho g_x$$

The common value selected for comparison was pressure drop. Both codes predicted the same pressure drop to four significant figures.

Table 1. Comparison of conservation equations from CTF and STAR.

Conservation Quantities	CTF		STAR	
	Inlet	Outlet	Inlet	Outlet
Mass – Mass Flow Rate (kg/s)	8.39	8.39	8.39	8.39
Energy - Power (MW)	11.7	11.7	11.7	11.7
Momentum – Pressure Drop (MPa)	16.06	15.99	16.06	15.99

2.2 Crossflow Magnitude in CTF and STAR

The magnitude of subchannel crossflow was examined in CTF and STAR to ensure similarity between codes. If STAR predicts a greater amount of crossflow than CTF, then crossflow is being calibrated in addition to Beta. The crossflow in CTF and STAR was identical with a range of +/- 0.002 m/s respectively. It is important to note that the directed crossflow model in CTF was not enabled during this analysis because the spacer grids are simple, non-mixing vane spacer grids (NVG).

3. CTF STEP 0: WEC EXPERIMENTAL DATA

The experimental data used throughout this analysis is from Westinghouse (WEC) non-mixing vane (NMV) grid, single bundle mixing experiments. NMV grids contain all the details of mixing vane grids (MVGs), but without the mixing vanes on top that are used to generate mixing in the bundle. A total of 23 mixing tests were performed for the bundle.

Figure 2 displays a cross-section of the rod bundle used during the experiments. The bundle is comprised of 5 NMV grids in the heated length with 36 subchannels and 25 rods in a 5x5 array. The 6 rods highlighted in red in Figure 2 are the hot rods. All of the rods are electrically heated, but the hot rods have a higher power than the other rods.

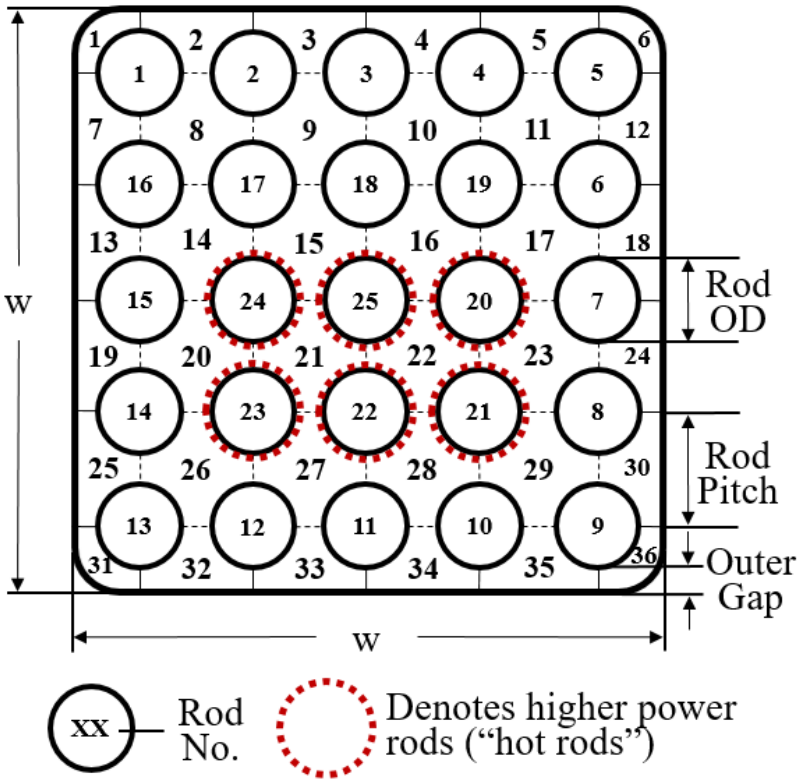

Figure 2. Cross-sectional geometry of the WEC NMV mixing experiments.

3.1 Mapping of Experimental Domain

The parameter ranges for the 23 NMV experiments provided by WEC are given in Table 2. Each column represents the data used to perform the CTF simulations.

Table 2. Experimental NMV data ranges from the 23 experiments provided by WEC.

	Test Section Exit Pressure (bars)	Test Section Inlet Temperature (°C)	Mass Velocity (kg/m²s)	Test Section Power (MW)
Minimum	101.333	213.031	2431.932	0.713
Maximum	164.765	312.441	3730.37	2.441

The pressure and temperature ranges from Table 2 were used to generate an experimental domain "box" (see Figure 3), where the experimental pressure range is represented on the x-axis and the experimental temperature range is represented on the y-axis. Based on the pressure range of the box, saturation temperature was determined and plotted with the box. Over this pressure range, saturation temperature (T_{sat}) behaves linearly as evidenced by the linear fit of T_{sat}. Experimental data points are plotted as yellow circles in Figure 3.

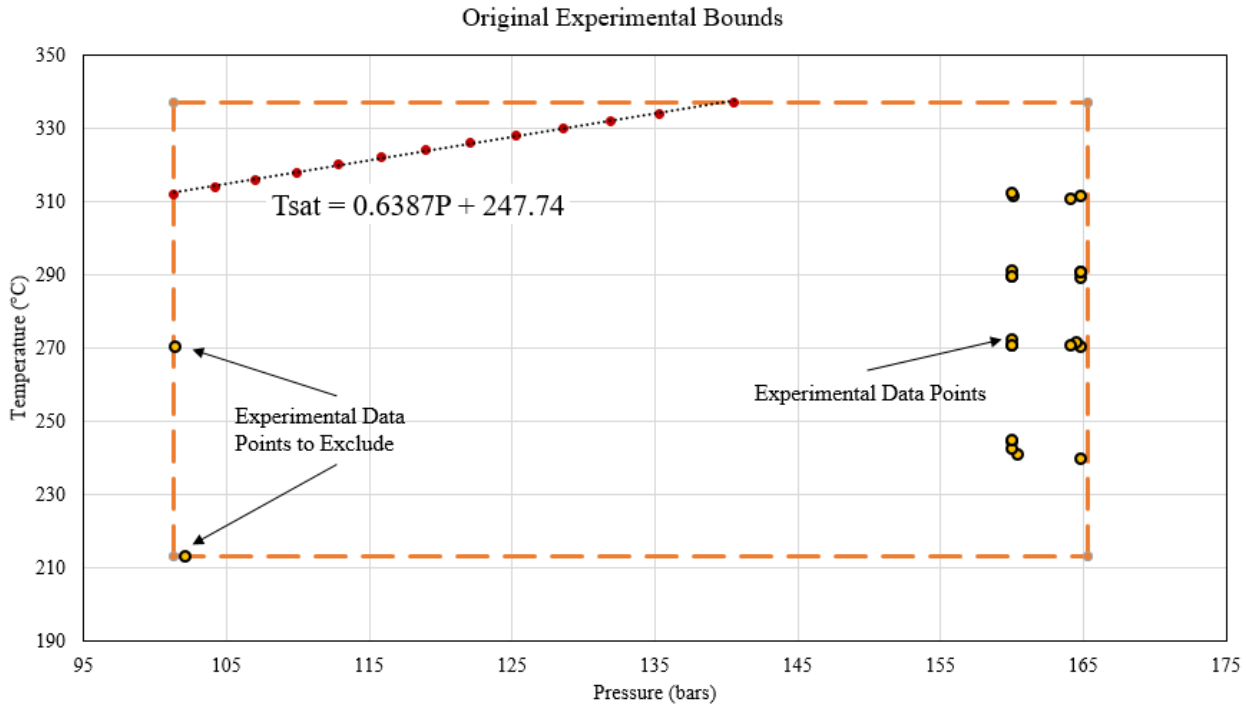

Figure 3. Map of experimental data using all data points.

The information in Figure 3 indicates that if the lower two experimental data points are used (where pressure is less than 105 bars), T_{sat} will intersect the bounds of the domain. This is an issue because STAR is a single phase code that does not recognize T_{sat}. Since 21 out of 23 data points are at higher pressures in the orange dashed domain, the two lower pressure tests were eliminated from the Hi2Lo process to ensure each of the test cases remains single phase.

The dark blue dotted box in Figure 4 demonstrate the new domain with the two low pressure tests eliminated (the old domain is plotted for reference). The T_{sat} line was also extended to demonstrate that T_{sat} does not intersect the new domain.

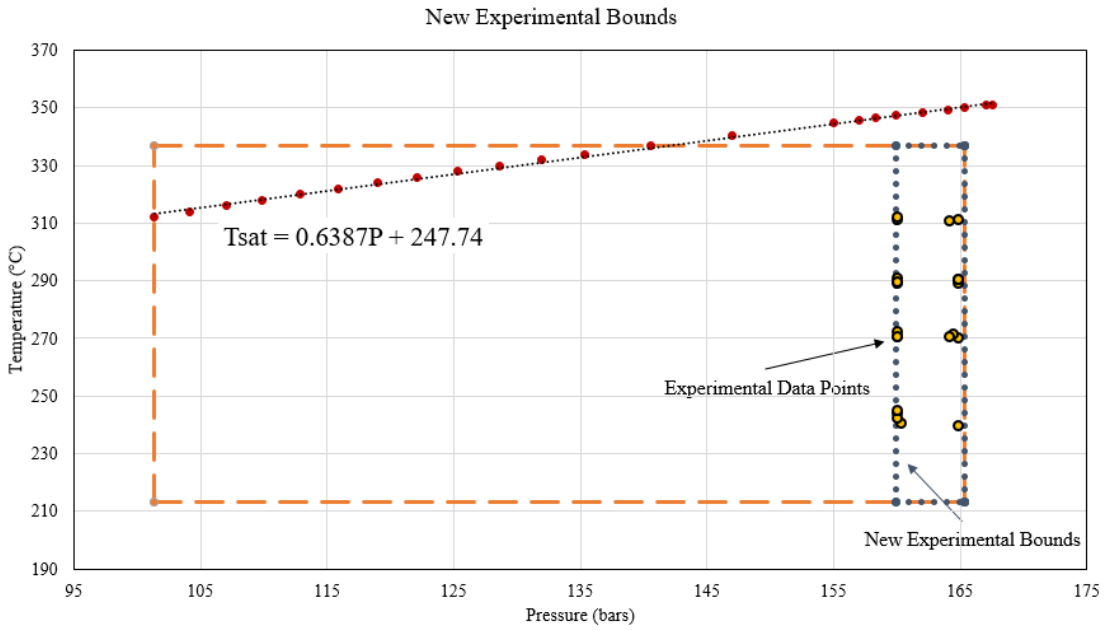

Figure 4. Map of experimental data excluding the low pressure points.

The new domain bounds were then increased 1% at a time to determine the maximum bounds for the Experimental Design step (CTF Step 5) without interfering with the T_{sat} line. CTF will allow for a 2% expansion of the new domain bounds without exceeding T_{sat}, but the bounds can only expand by 1% when taking into consideration the change in temperature from the center of the subchannel to the rod surface in STAR (see Figure 5-2 in Reference 1). The 1% expanded bounds are given in Figure 5 by the light blue dot/dash line.

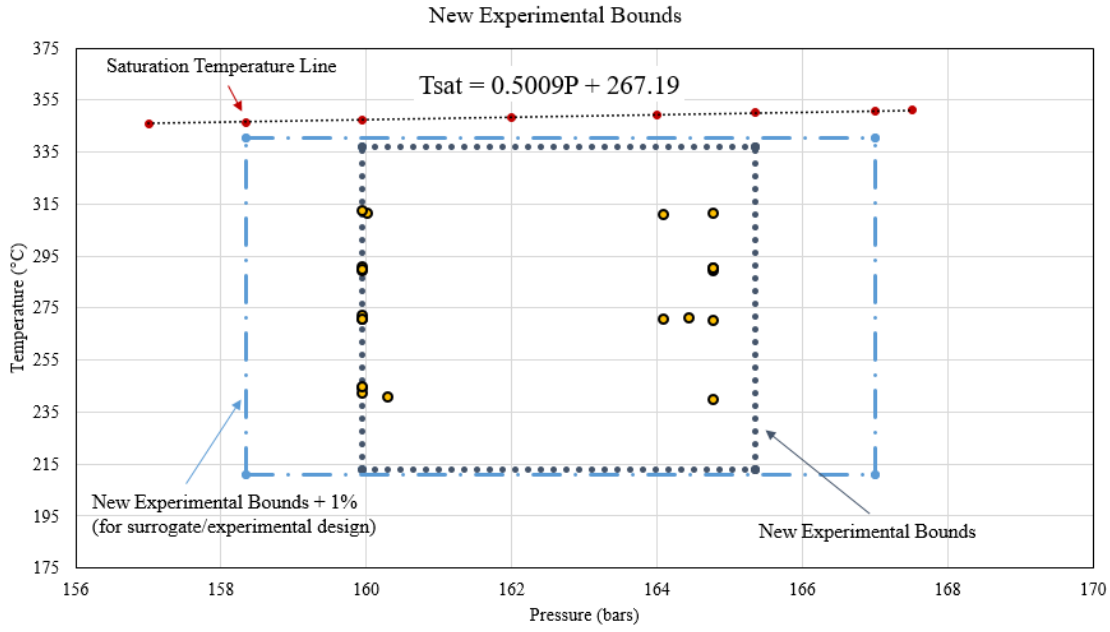

Figure 5. Map of experimental data excluding the low pressure points and the 1% expanded bound that will be used for determining the Experimental Design points.

3.2 Experimental Data Splitting

The experimental data in Table 2, except the two low pressure tests, were split into two representative sets. The range of the first set, given in Table 3, consists of 10 tests and was used exclusively for validation.

Table 3. CTF Validation data set ranges for each parameter contributing to CTF input.

	Test Section Exit Pressure (bars)	Test Section Inlet Temperature (°C)	Mass Velocity (kg/m²s)	Test Section Power (MW)
Minimum	159.939	240.974	2438.878	0.916
Maximum	164.765	311.573	3730.37	2.102

The range of the second set of experimental data, provided in Table 4, is comprised of 11 tests which were set aside for calibration.

Table 4. CTF Calibration data set ranges for each parameter contributing to CTF input.

	Test Section Exit Pressure (bars)	Test Section Inlet Temperature (°C)	Mass Velocity (kg/m²s)	Test Section Power (MW)
Minimum	159.939	239.848	2431.932	0.919
Maximum	164.765	312.441	3688.146	2.441

3.3 Generating Polynomials for STAR Inlet Fluid Conditions

In order to ensure STAR and CTF are operating at the same fluid conditions throughout this process, CTF fluid properties were used to generate functions to define STAR fluid properties. STAR uses polynomial functions that are fit to fluid property data. To ensure that CTF and STAR use the same fluid properties, polynomials were generated from CTF fluid property output. In the master branch version of CTF, there are two options for designating fluid property tables: Original CTF property tables (mix of various sources) and IAPWS IF97 tables[2]. The IAPWS IF97 tables were selected for use in this milestone because the source of the tables is well known and accessible outside of CTF.

The IAPWS IF97 fluid property data is not fully accessible without modifying the CTF source code. A write statement was placed at the beginning of `Result_channel_mod.f90` to extract fluid properties from the `liquid_props` subroutine over a specific pressure and enthalpy range and write the results to a text output file.

The properties needed to fully define the fluid in STAR include density, specific heat, thermal conductivity, and dynamic viscosity. Fluid properties were evaluated over a pressure range of 158.34 bar to 166.998 bar, representing 1% less than the minimum exit pressure and 1% more than the maximum inlet pressure respectively to ensure there is no extrapolation outside of the observed range. This pressure range was divided into 20 isobars and property data were printed over a temperature range of 484 K to 613 K for each isobar. The lower bound temperature is 1% lower than

the minimum inlet temperature of all the experimental tests and the upper bound temperature is 1% higher than the maximum experimental outlet temperature of all the tests. Given that the pressure range for the experimental domain is less than 10 bars, therefore not contributing a significant change in fluid property values, pressure is assumed a constant for purposes of polynomial generation. A single polynomial was therefore fit to all 20 isobars.

Fits for each of the fluid properties are fourth order polynomials to ensure a tight fit to the fluid data inside the selected temperature range. While there is a chance that fitting to such a high order could result in higher error outside the specified range, the properties are well behaved below saturation and the fluid conditions of the analysis should remain within the specified temperature bounds. The polynomial fits for density, specific heat, thermal conductivity, and dynamic viscosity are given in Figures 6, 7, 8, and 9 respectively.

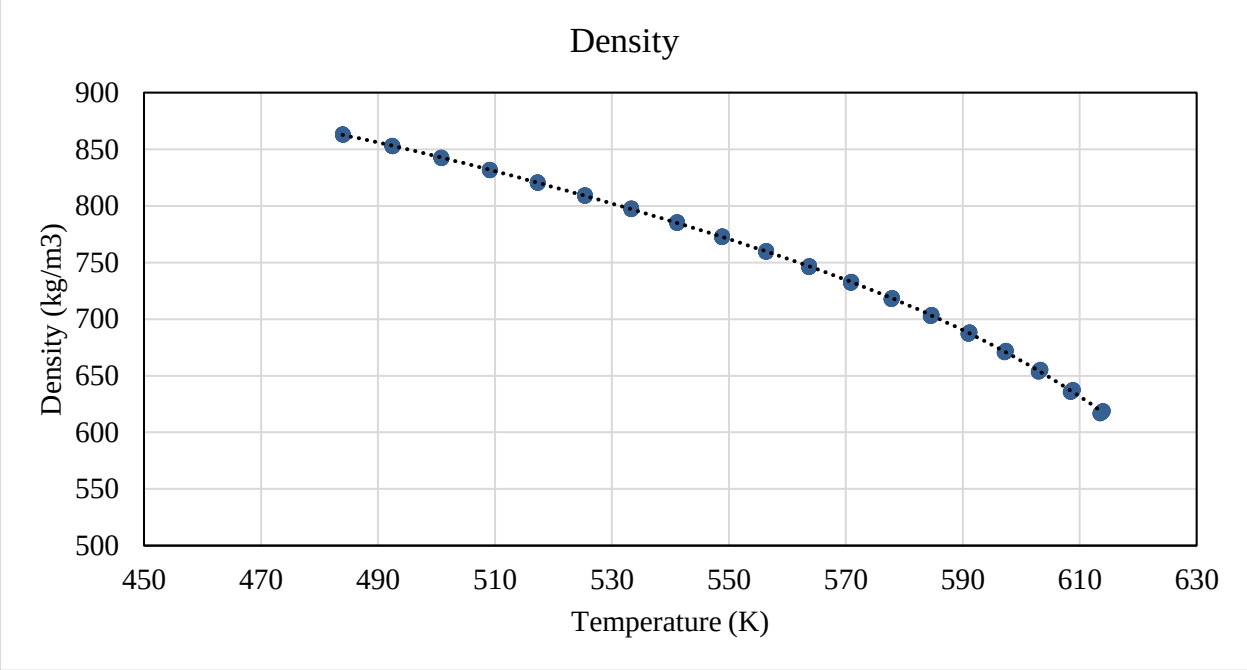

Figure 6. Polynomial density function generated from a fit over 20 CTF IAPWS IF97 isobars.

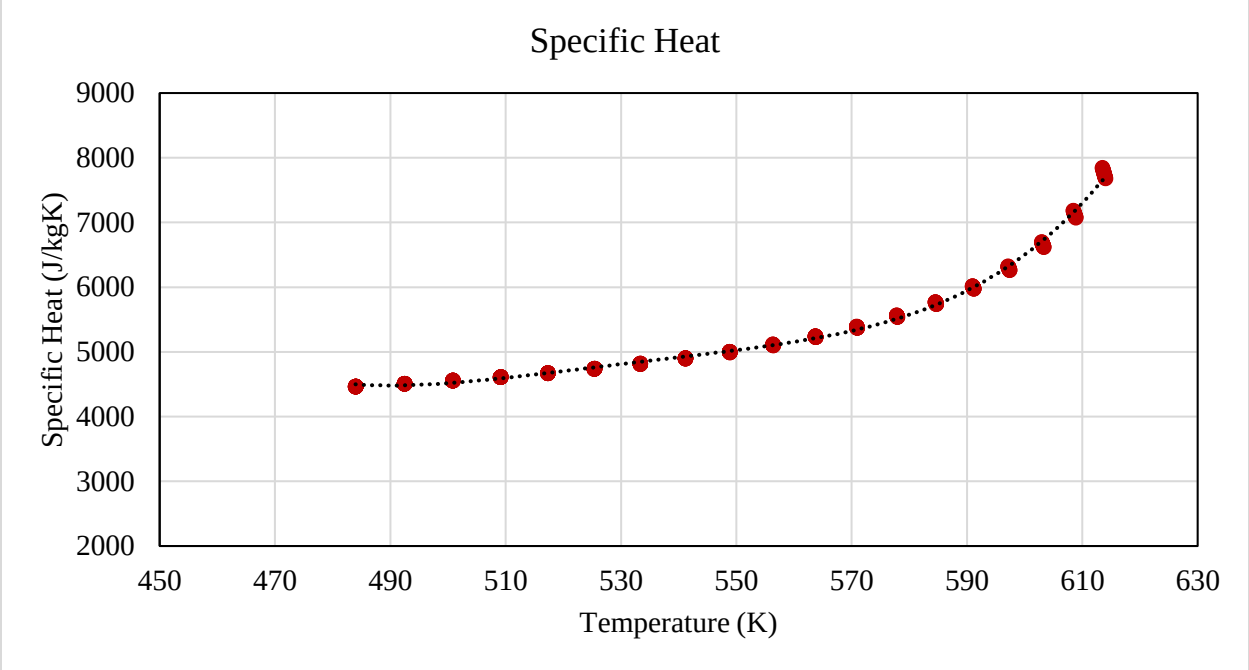

Figure 7. Polynomial specific heat function generated from a fit over 20 CTF IAPWS IF97 isobars.

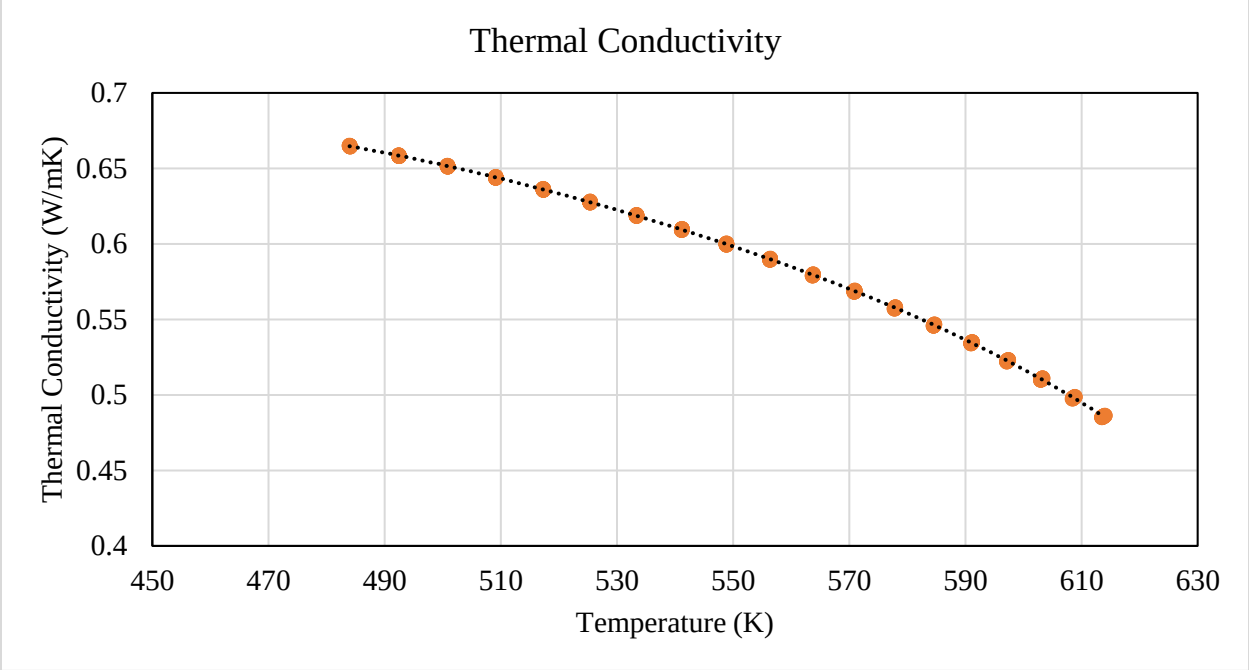

Figure 8. Polynomial thermal conductivity function generated from a fit over 20 CTF IAPWS IF97 isobars.

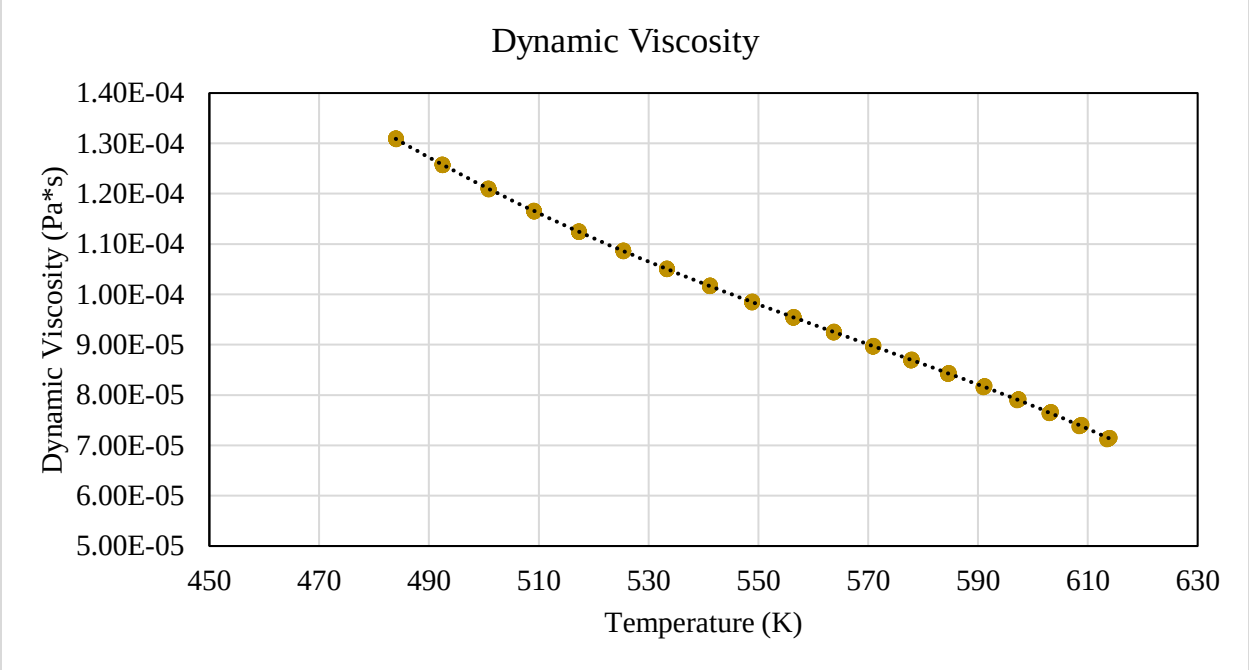

Figure 9. Polynomial dynamic viscosity function generated from a fit over 20 CTF IAPWS IF97 isobars.

For each of the polynomial fits, six decimal places were expressed in the coefficients. Without this level of precision, the polynomials produced significantly different fluid properties from the CTF generated fluid property data points. The polynomials for each of the fluid properties used as STAR input are provided in Table 5, where ρ is density, c_p is specific heat, k is thermal conductivity, and v is dynamic viscosity.

Table 5. Polynomials used to define fluid properties in STAR for this analysis.

Fluid Properties	Polynomial Fits (STAR Input)
Density	$\rho = -5.408416e^{-7}(T^4) + 1.132377e^{-3}(T^3) - 8.923019e^{-1}(T^2) + 3.121676e^{2}(T) - 3.990909e^{4}$
Specific Heat	$c_p = 4.277308e^{-5}(T^4) - 9.077996e^{-2}(T^3) + 7.223995e^{1}(T^2) - 2.553508e^{4}(T) + 3.386247e^{6}$
Thermal Conductivity	$k = -2.345491e^{-10}(T^4) + 4.936334e^{-7}(T^3) - 3.936989e^{-4}(T^2) + 1.398904e^{-1}(T) - 1.791301e^{1}$
Dynamic Viscosity	$v = -3.398248e^{-14}(T^4) + 6.255825e^{-11}(T^3) - 4.080035e^{-8}(T^2) + 1.031840e^{-5}(T) - 5.335271e^{-4}$

Verification of the polynomials was performed by selecting seven different isobars within the pressure bounds and printing IAPWS IF97 fluid properties from CTF over the temperature range of the polynomials. The temperature values were plugged into each of the fluid property polynomials and plotted against the fluid property values from CTF. The results of this test, given statistically in Table 6 and visually in Figures 10-13, display reasonable agreement between the CTF fluid property values and those predicted using the polynomials. The L_2 norms for each fluid property were calculated using the following equation:

$$L_{2,CTF/Polynomial} = \frac{\sqrt{\sum_{i=1}^{133}(CTF - Polynomial)^2}}{\sqrt{\sum_{i=1}^{133} CTF^2}}$$

where CTF refers to the ith CTF fluid property value and $Polynomial$ is the ith fluid property value predicted by each polynomial. Note, 133 data points were used to construct each of the four fluid property polynomials.

Table 6. Difference in fluid properties between CTF and polynomial generated from CTF fluid properties quantified using L_2 norms.

	L_2 Norms
Density	0.0009
Specific Heat	0.0074
Thermal Conductivity	0.0008
Dynamic Viscosity	0.0011

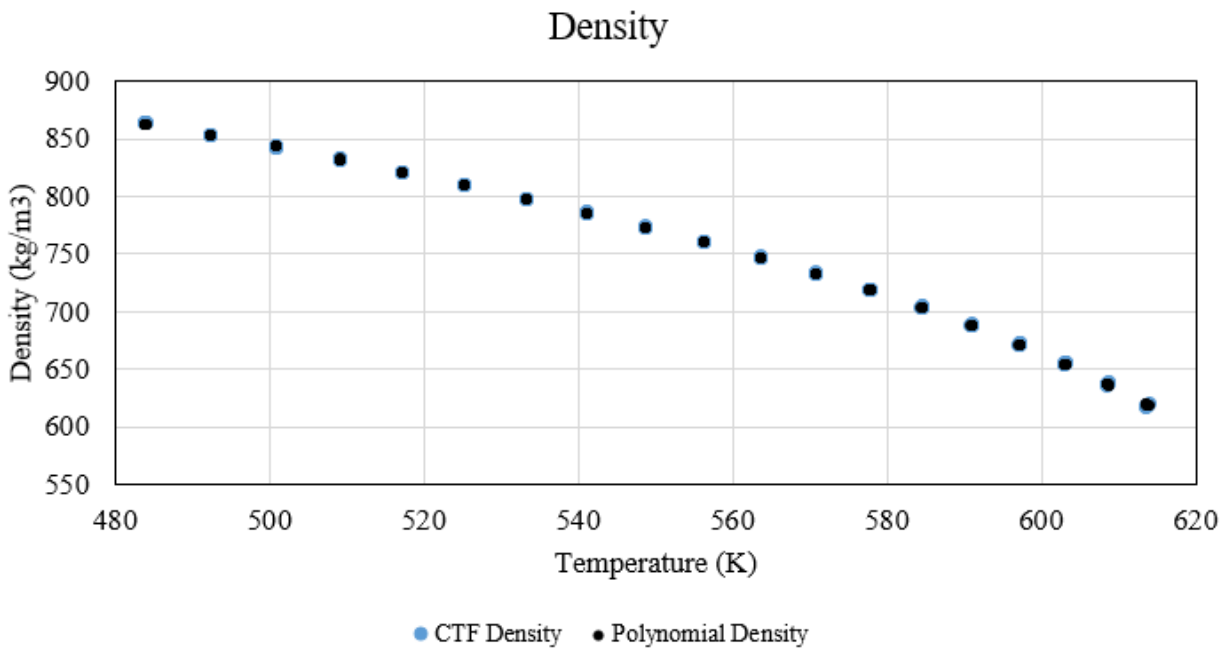

Figure 10. Test of polynomial density function with 7 isobars not used to train polynomial.

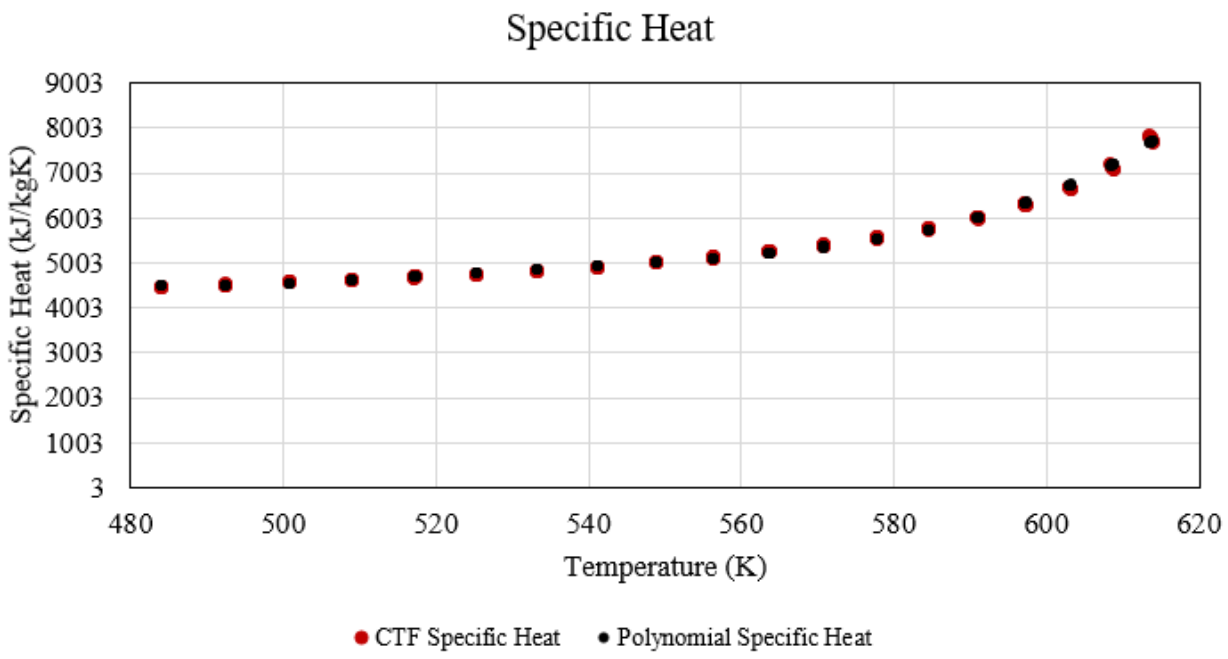

Figure 11. Test of polynomial specific heat function with 7 isobars not used to train polynomial.

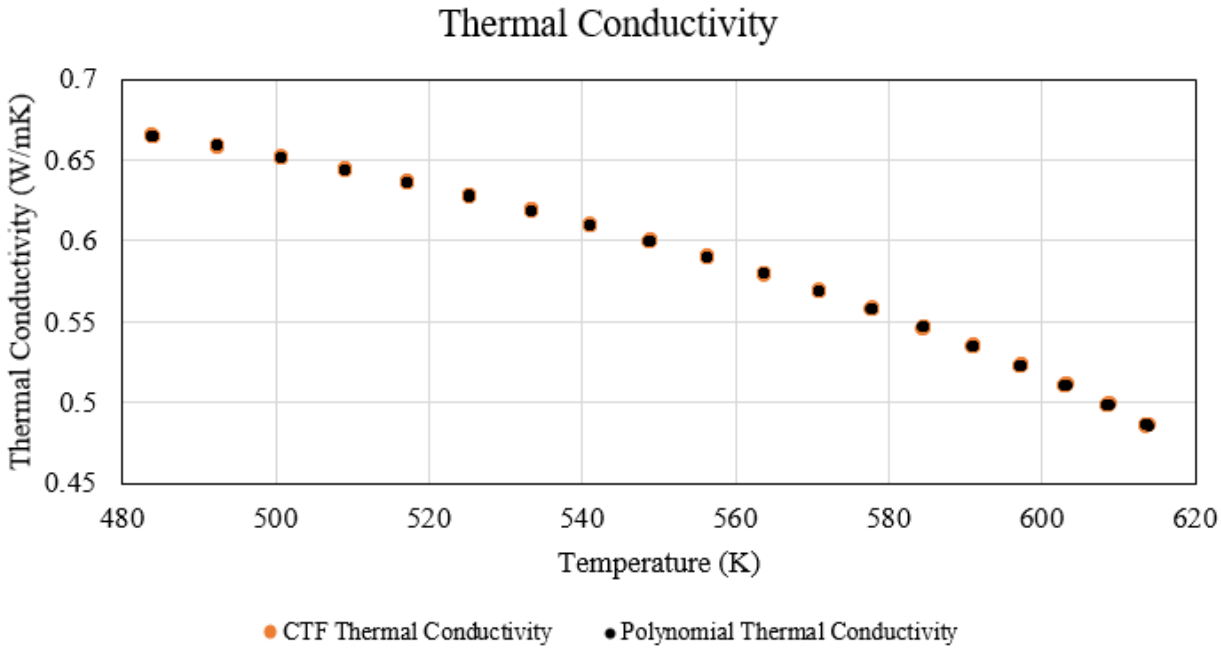

Figure 12. Test of polynomial thermal conductivity function with 7 isobars not used to train polynomial.

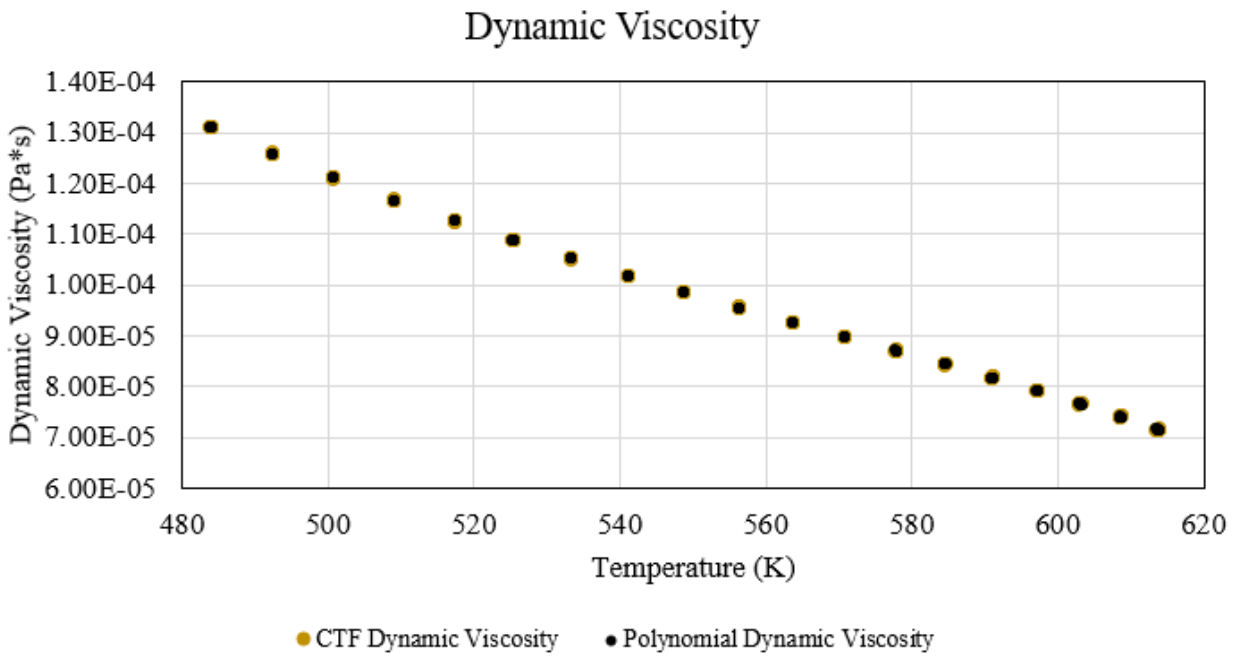

Figure 13. Test of polynomial dynamic viscosity function with 7 isobars not used to train polynomial.

4. CTF STEP 1: INITIAL QUANTITATIVE VALIDATION OF CTF

The experimental test conditions referenced in Table 3 were used to perform an initial quantitative validation of CTF. For this initial validation, the CTF mixing coefficient, Beta, was set to a value of 0. A Beta value of 0 means no mixing occurs between subchannels in the bundle. In the case of the NMV geometry, this means that there are no mechanisms for crossflow or mixing when Beta is set to 0. The calibration steps performed after validation will be used to tune Beta to provide the level of mixing seen in the experiment and STAR.

The quantity of interest throughout this work is subchannel average outlet temperature. To quantify the distance in subchannel outlet temperatures between CTF and the experimental data, L_2 norms were calculated at each validation step. The formulation of the L_2 norm used for individual tests throughout this work to compare CTF to the experiment is:

$$Individual\ Test\ L_{2,EXP/CTF} = \frac{\sqrt{\sum_{i=1}^{36}(EXP - CTF)^2}}{\sqrt{\sum_{i=1}^{36} EXP^2}}$$

and the overall L_2 norm was calculated using the equation:

$$Overall\ L_{2,EXP/CTF} = \frac{\sqrt{\sum_{i=1}^{360}(EXP - CTF)^2}}{\sqrt{\sum_{i=1}^{360} EXP^2}}$$

where EXP refers to the ith experimental subchannel outlet temperature and CTF is the ith CTF subchannel outlet temperature. The L_2 norm between CTF and the experiment was normalized by the L_2 norm of the experiment to allow the distance between temperatures to be in presented in non-

dimensional form. L_2 norms were calculated for each validation experimental test as well as overall for the 10 validation tests. The results of these calculations are given in Table 7.

Table 7. Initial validation L_2 results for each individual test as well as the overall L_2 norm.

Test Number	Initial Validation (Beta = 0)
1	0.01235
2	0.01351
3	0.01369
4	0.01279
5	0.01378
6	0.01093
7	0.01396
8	0.01405
9	0.01660
10	0.02223
Overall L_2	0.0144

The L_2 norms for each individual test are between 1% and 2.2%, while the overall L_2 norm is 1.4%. This indicates statistically that CTF outlet temperatures are about 1.4% different than the experimental outlet temperatures. This does not leave much room for improvement during the calibration process, but some improvement is possible.

Figure 14 provides a graphical representation of the CTF initial quantitative validation results. CTF outlet temperature was plotted against the outlet temperature measured in the experimental tests. The black dotted line represents the ideal condition where the CTF outlet temperatures are 0% different from the experimental outlet temperatures. The red lines depict the actual percent difference bounds of the CTF points (which are given as blue circles).

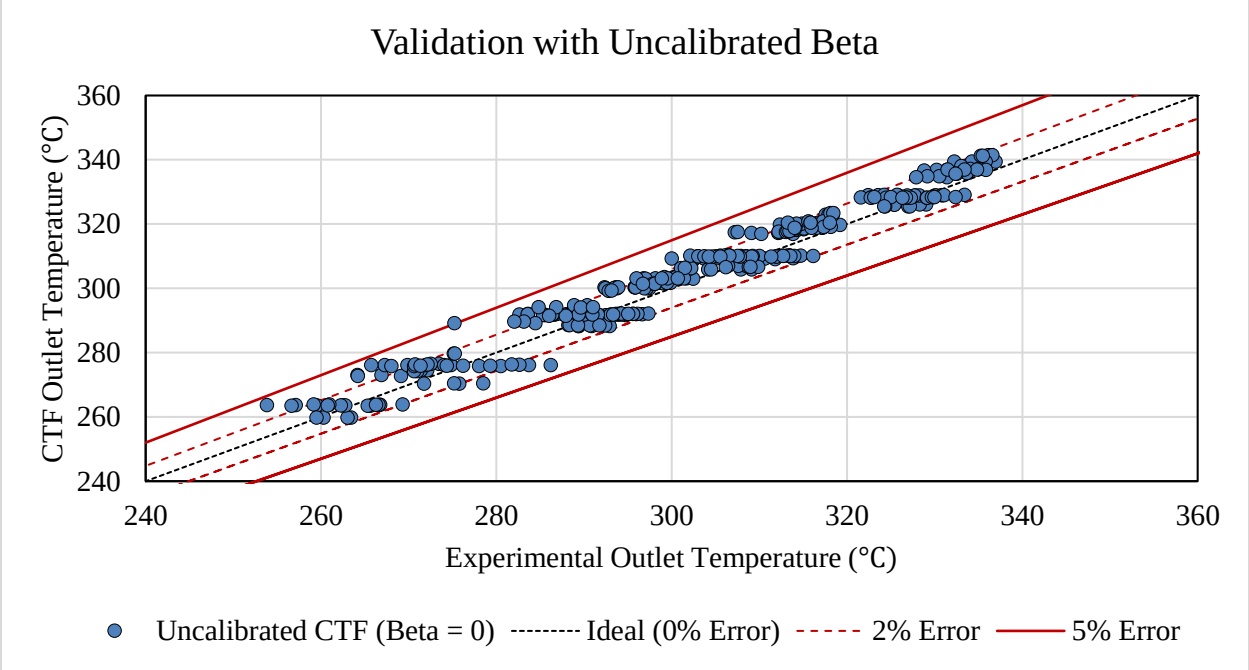

Figure 14. Results of the validation study between CTF outlet temperatures, with Beta equal to 0, and the outlet temperatures of the validation experiments. The CTF outlet temperatures were within 5% of the experimental outlet temperatures.

The difference between the CTF outlet temperatures and the experimental outlet temperatures is within a few percent in the graphical representation as well. As expected when considering all 36 points of the 10 validation tests, the difference is larger than the overall 1.4%, however most of the points fall within the 2% difference bounds. This means that the calibration of Beta will not result in a dramatic improvement in the CTF outlet temperatures with respect to the experiment, but some improvement could occur.

5. CTF STEP 2: SURROGATE CONSTRUCTION

For this geometry and application, CTF simulations completed on the order of approximately five minutes. While this is much less computationally expensive than the hour it takes to run the same geometry and flow conditions in STAR, the computational time adds up for the Bayesian calibration and Experimental Design steps. On the order of 10^4 runs were needed for each Bayesian calibration, therefore building a surrogate of the CTF simulation was necessary. The surrogate used in this work completed a run within seconds verses the five minutes it took to run a simulation in CTF.

5.1 Build Surrogate

The surrogate bounds are identical to those described in Figure 5 of CTF Step 0, 1% lower and higher than the minimum and maximum experimental conditions for all of the configuration variables. The configuration variables, model parameters that change between experiments, include exit pressure, inlet temperature, inlet mass flow rate, and average linear heat rate per rod (AFLUX). As stated previously, the calibration parameter for this study is Beta, which was allowed to vary between 0 and 0.012 (twice the WEC-predicted nominal value). It is important to specify the same ranges on the calibration and configuration variables throughout the surrogate construction process to ensure evaluation and use of the identical surrogate is performed. The method used to construct a surrogate for the purposes of this study includes four steps:

a) Generate a Latin Hypercube Sampling (LHS) design to use for surrogate training and run the low-fidelity code (CTF in this study) on this design
b) Generate a LHS design to use for surrogate testing (validate and run the low-fidelity code, CTF this study) on this design
c) Build the surrogate using the training design
d) Evaluate the surrogate on the test design

Steps a) and b) were performed using the Latin Hypercube Sampling method block in Dakota. The only Dakota input differences between steps a) and b) were the random seed used to select the LHS points and the number of samples, 1,000 for the design verses 300 for the testing. Changing the random seed number insures the independence of the two sets of LHS data produced in the two steps.

Step c) is the step in the process where the surrogate is generated. Through model specification in Dakota, the LHS design points from Step a) are read in and used to build the Gaussian Process (GP) surrogate. Ideally, Predictive Residual Error Sum of Squares (PRESS) statistics would be specified in the same Dakota model block as the surrogate, however, due to the time constraints of this analysis, PRESS statistics were not performed. With PRESS statistics computed, Dakota reads in the LHS testing points from Step b) and outputs surrogate quality metrics, but this process can take weeks to build a surrogate. Without using PRESS, the surrogate builds in approximately 20 minutes.

The process used to perform Step d) for this analysis, without PRESS turned on, is described in the next section.

5.2 Test Surrogate with CTF

In lieu of using PRESS statistics to evaluate the quality of the surrogate created in Step c), the 300 testing points generated in Step b) were used to test how closely the surrogate predicts CTF results. The surrogate was also evaluated at the same 300 testing points as CTF, Step c, and outlet temperatures were compared to the CTF outlet temperatures collected during Step b) using L_2 norms. The formulation of the L_2 norm used in this portion of the analysis was:

$$L_{2,SURR/CTF} = \frac{\sqrt{\sum_{i=1}^{36}(CTF - SURR)^2}}{\sqrt{\sum_{i=1}^{36} CTF^2}}$$

where $SURR$ represents the ith subchannel temperature calculated by the surrogate. The L_2 comparison between CTF and the Dakota-generated surrogate are given in Figure 15.

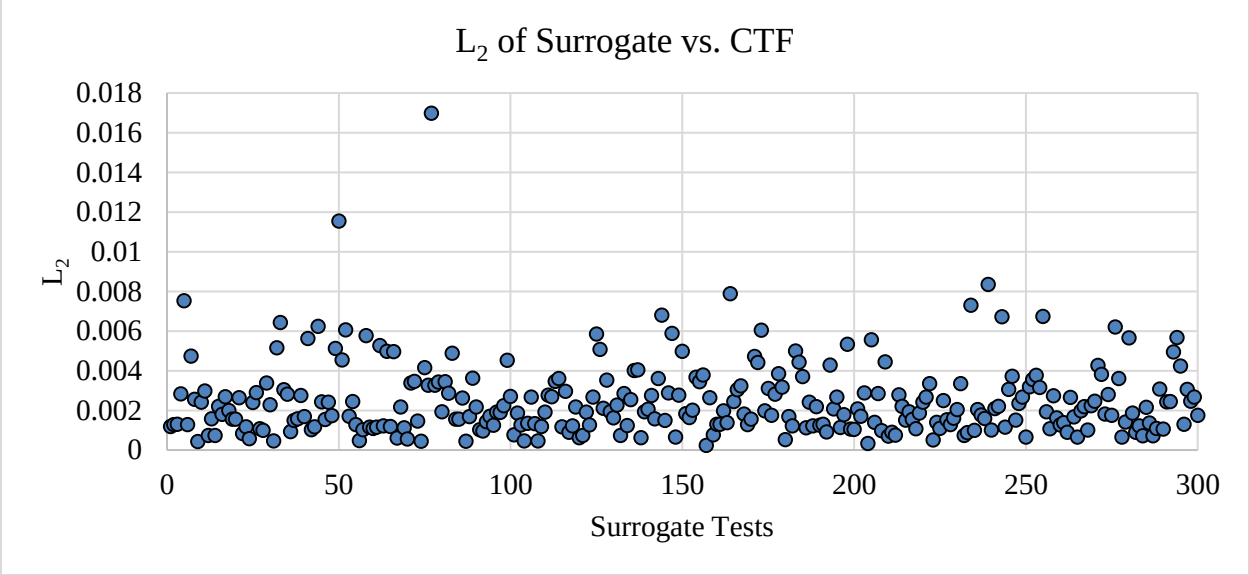

Figure 15. L_2 comparison between CTF and the surrogate built in Step c) for each of the validation tests. Note, the test numbers in the experiment are not fully sequential, which is why there is a gap in the experimental test number.

The difference between the surrogate-calculated and CTF outlet temperatures for each of the validation test conditions is less than 1.8% with the differences for most of the tests being within 0.02-0.6%. Based on these results, the surrogate was considered to adequately model CTF for the purposes of this analysis.

6. CTF STEP 3: BAYESIAN CALIBRATION WITH SURROGATE

Bayesian calibration using the surrogate from CTF Step 2 was performed four times to determine how many of the experimental tests would be used as the priors during Bayesian calibration. The first calibration used a single experimental test, the second used two experimental tests, the third incorporated three experimental tests, and the fourth included all experimental calibration tests (11 total tests). For each calibration, 11,000 MCMC chain samples were collected with the intention of discarding the first 1,000 to account for burn-in. A Kernel Density Estimation (KDE) was calculated from the last 10,000 MCMC chain samples of Beta for each of the Bayesian calibrations to determine how many experimental data points should be used in the initial Bayesian calibration as well as Experimental Design step. The resulting KDEs are presented in Figure 16.

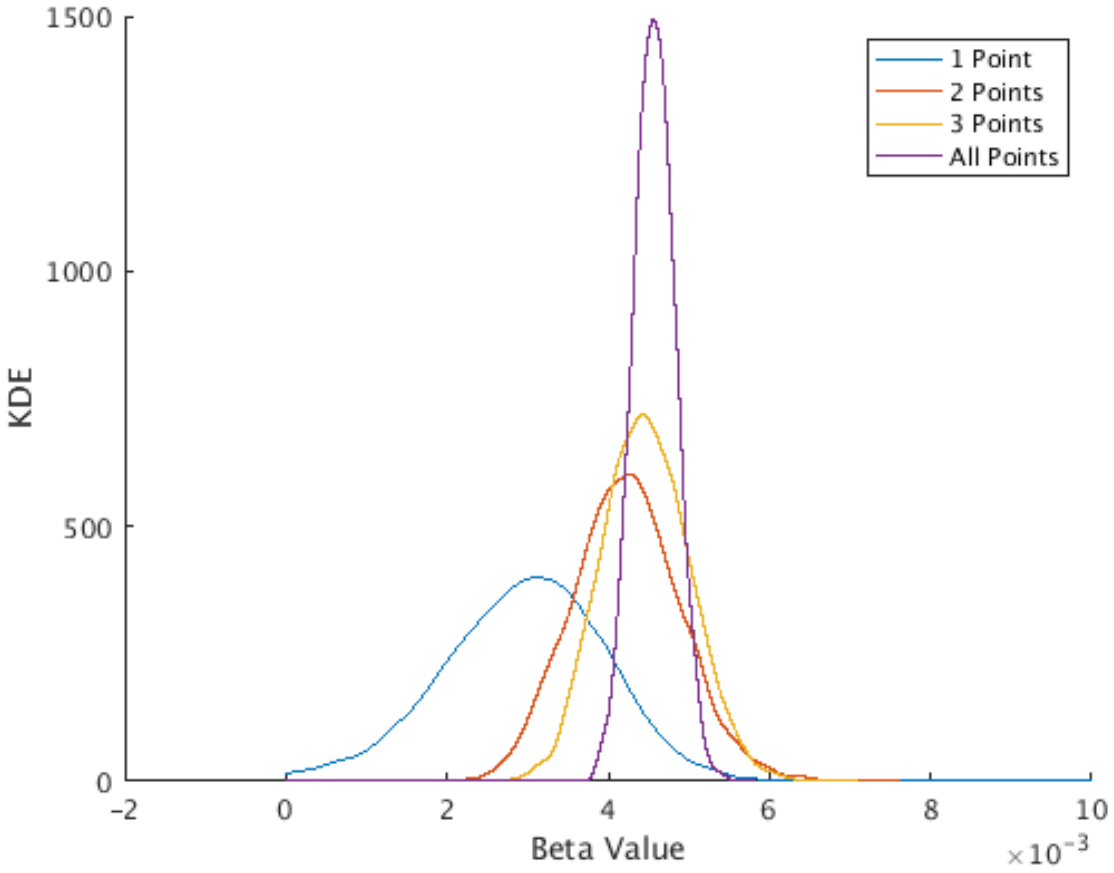

Figure 16. Kernel Density Estimation (KDE) of the MCMC results from Bayesian Calibration using one experimental data calibration point, 2 experimental data calibration points, 3 experimental data calibration points, and all experimental data calibration points.

As the number of experimental tests included in the Bayesian calibration increases, the distribution on the optimal value of Beta narrows with a taller peak. A decision was made to use the one experimental data point instead of all calibration data points to allow more room for improvement in the value of Beta through the Experimental Design (CTF Step 5) process. Ideally, more experimental points would be used in an initial calibration, however, this problem is not highly sensitive to changes in Beta. For the purposes of fully demonstrating the Hi2Lo process, less experimental data points were used with the expectation that more improvement in Beta optimal would be gained during the remaining portion of the Hi2Lo process.

Using the one experimental data point, the first Bayesian calibration yielded an optimal Beta value of 0.003197. A check of the optimal value of Beta was performed and described in the next section.

6.1 Check of Beta Optimal with CTF

Three CTF runs were performed using the optimal value identified from Bayesian calibration, 0.003197, as well as one standard deviation above, 0.002205, and below, 0.004188, the optimal value. The expectation is that the optimal Beta value from the calibration step should yield outlet temperatures closer to the experimental data than when values above and below the optimal Beta value are used. The L_2 norm results of these three runs are provided in Figure 17.

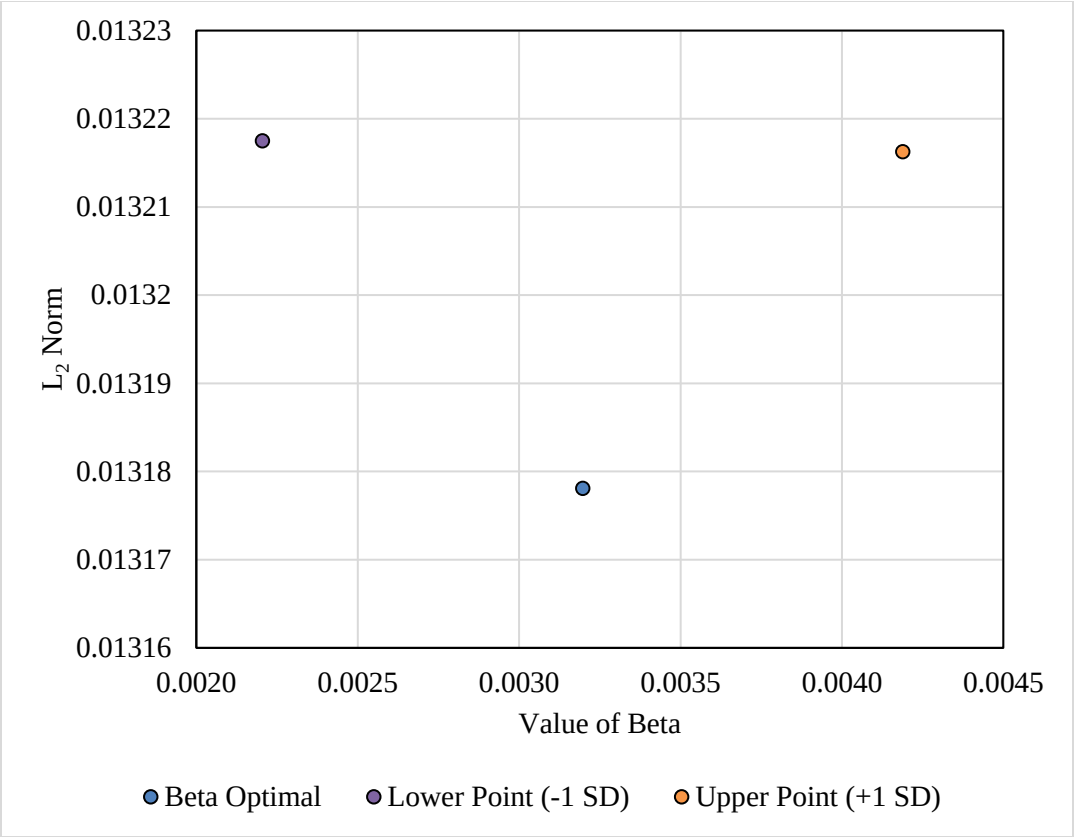

Figure 17. L_2 norm results of a check to determine if the optimal value of Beta determined during Bayesian calibration produces outlet temperatures that are closer to the experimental outlet temperatures (lower L_2 norm) than Beta values above and below.

The L_2 norm for Beta optimal in Figure 17 is lower than the norms for Beta optimal plus/minus one standard deviation. Since the Beta optimal simulation produces outlet temperatures with a lower L_2 norm than lower or higher values of Beta, this test provided confidence that the surrogate identified a reasonable value of Beta optimal. If the simulation using the Beta optimal value from the Bayesian calibration using a surrogate had yielded outlet temperatures further away from the experimental temperatures, the surrogate would need to be rebuilt to better reflect the behavior of CTF.

7. CTF STEP 4: 2ND QUANTITATIVE VALIDATION

A second validation step was performed to determine the improvement with respect to the experimental data outlet temperatures when changing Beta from 0 to 0.003197. Table 8 provides a side by side comparison of the individual test L_2 norms using a Beta of 0 and Beta of 0.003197 as well as comparing overall L_2 values from each validation. The formulation of the L_2 norm used for individual tests throughout this work to compare CTF to the experiment is:

$$Individual\ Test\ L_{2,EXP/CTF} = \frac{\sqrt{\sum_{i=1}^{36}(EXP - CTF)^2}}{\sqrt{\sum_{i=1}^{36} EXP^2}}$$

and the overall L_2 norm was calculated using the equation:

$$Overall\ L_{2,EXP/CTF} = \frac{\sqrt{\sum_{i=1}^{360}(EXP - CTF)^2}}{\sqrt{\sum_{i=1}^{360} EXP^2}}$$

where EXP refers to the ith experimental subchannel outlet temperature and CTF is the ith CTF subchannel outlet temperature.

Table 8. L_2 norm comparison, for each experimental test and overall, between the initial validation with a Beta value of 0 and the second validation that was performed after Bayesian Calibration identified a Beta optimal value of 0.003197.

Test Number	Initial Validation (Beta = 0)	2nd Validation (Beta = 0.003197)
1	0.01235	0.01144
2	0.01351	0.01342
3	0.01369	0.01292
4	0.01279	0.01247
5	0.01378	0.01318
6	0.01093	0.01079
7	0.01396	0.01309
8	0.01405	0.01295
9	0.01660	0.01596
10	0.02223	0.01997
Overall L_2	**0.0144**	**0.0136**

The overall L_2 value decreased by approximately 0.001 (0.1%) when using a Beta calibrated with one experimental test. When looking at the L_2 norms of each validation test, approximately the same decrease was observed. In an ideal application of the Hi2Lo process, a larger improvement in the L_2 norm would be expected. One reason this application does not experience a larger improvement is the lack of strong sensitivity due to changes in the Beta coefficient in CTF.

A graphical representation of Table 8 is given in Figure 18.

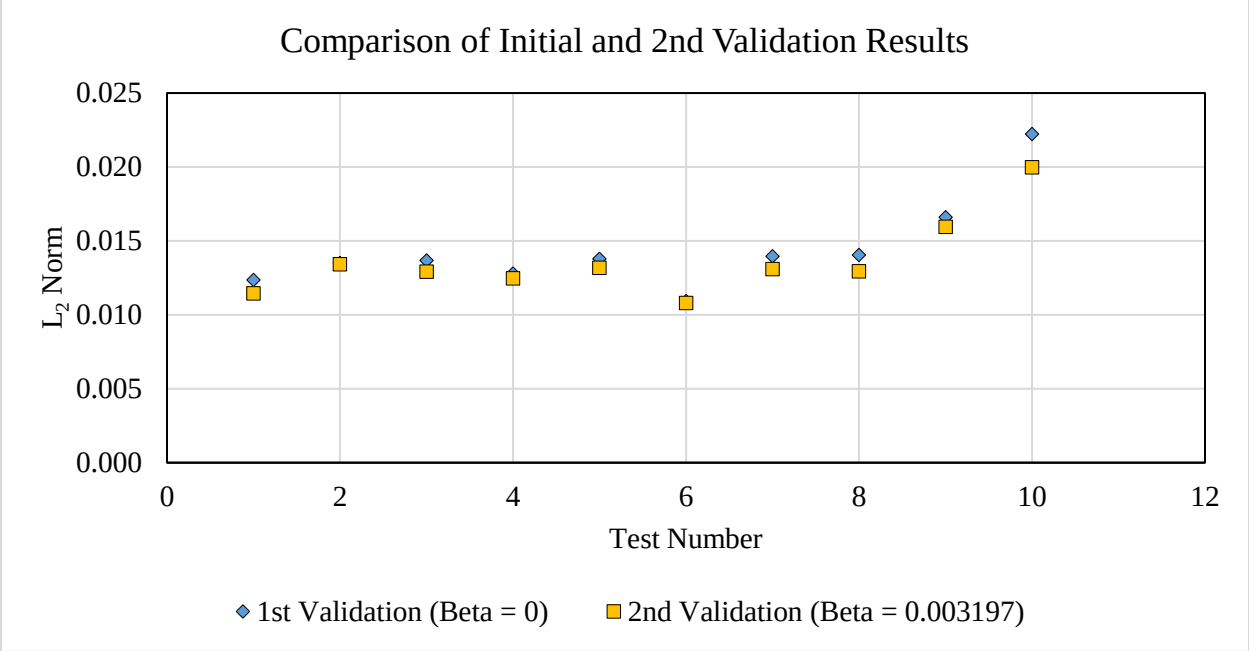

Figure 18. Graphical comparison of the L_2 values from the initial validation compared to the L_2 values from the second validation.

Figure 18 indicates that some improvement was made, but the scale on the y-axis is small. The expectation is that through an Experimental Design process, further improvements in Beta optimal will occur to more closely align the CTF outlet temperatures with the experimental outlet temperatures. This is because adding more data points to the calibration will reduce the uncertainty in Beta optimal.

8. CTF STEP 5: EXPERIMENTAL DESIGN AND BAYESIAN CALIBRATION WITH SURROGATE

The Experimental Design process commenced by providing Dakota with a list of candidate points, the LHS design used in the Bayesian calibration (CTF Step 3), and a calibration data file. The list of candidates for this analysis was comprised of the experimental test conditions provided by WEC. The first line in the calibration data file contained outlet temperatures from one of the experimental tests as well as the associated experimental standard deviations (1.667 °C).

The first iteration is a Gaussian process using the surrogate to determine where the high-fidelity simulation should be evaluated. For each iteration, Dakota outputs a file called experimental_design_output.txt that contains the optimal design of the configuration variables and its estimated mutual information. The optimal design is then passed to the high-fidelity simulation for evaluation. It is important to change the random seed in the Bayesian calibration method block for each Experimental Design iteration to preserve independence of the results.

The Experimental Design process was performed once using STAR outlet temperatures as the high-fidelity simulation and again using experimental outlet temperature data as the high-fidelity simulation. The purpose was to determine if using the experimental temperatures as high-fidelity results would yield the same outcome as using STAR for high-fidelity results.

Since STAR runs are expensive, the passing of information between Dakota and STAR was performed offline as a manual process. The functionality to perform this analysis inline, allowing Dakota to drive the high-fidelity simulation runs, is currently in Dakota 6.6 and could be implemented for problems with less intensive high-fidelity codes.

Once the high-fidelity run is complete at the optimal design, the outlet temperatures are passed back to Dakota. For the manual process described in this work, the high-fidelity outlet temperatures would be inserted on the next line of the calibration data file along with the configuration variables used to obtain the data and the variances of the data.

Since it is not believed that the results from STAR are physical truth because they do not account for uncertainties found in physical reality, noise was added to the STAR results to better reflect the true uncertainties that could not be captured in the limited Uncertainty Quantification that was performed. Noise was added to the STAR outlet temperatures based on randomly sampling a Gaussian distribution to account for the fact that the experimental outlet temperatures are inherently noisy, whereas the STAR outlet temperatures are not. This process is described in the next section.

8.1 Adding Noise to STAR Outlet Temperatures to Approximate Experimental Noise

An Uncertainty Quantification (UQ) study was performed in STAR using six different conditions (see STAR Step 2 in Reference 1). The outlet temperature results were organized into a text file where each column represents one of the 36 subchannels (random variables) and each row represents one observation. The 6 by 36 matrix formed by the UQ results was used to calculate a covariance matrix with size 36 by 36. The resulting subchannel variances were two orders of magnitude smaller than the experimental variances, so the covariance matrix was multiplied by 100 to approximate the same magnitude of noise as the experiment. A diagonal matrix was formed using the diagonal elements of the original matrix.

Simulated noise was determined for each Experimental Design iteration by selecting 20 random samples of a multivariate Gaussian distribution with a mean of zero and using the calculated diagonal covariance matrix. This process resulted in a 20 by 36 array of errors (noise). The *n*th set of errors were added to the *n*th iteration of STAR outlet temperatures generated by running each optimal design.

The STAR variance per subchannel obtained from the STAR UQ step was scaled in a similar fashion to the noise. To obtain standard deviations on the same scale as the experiment, the 36 STAR variances were multiplied by 100. This results in a standard deviation that is 10 times larger than the STAR standard deviation.

8.2 Experimental Design and Calibration Results

The initial Experimental Design process was performed as planned, using STAR outlet temperatures as high-fidelity results. The first line of the calibration data file was seeded with the experimental outlet temperatures from one of the calibration tests as a prior for Dakota. The list of candidates was the 21 STAR validation runs minus the test used as the prior. The Experimental Design process took 20 iterations to complete. The mutual information per iteration is given in Figure 19.

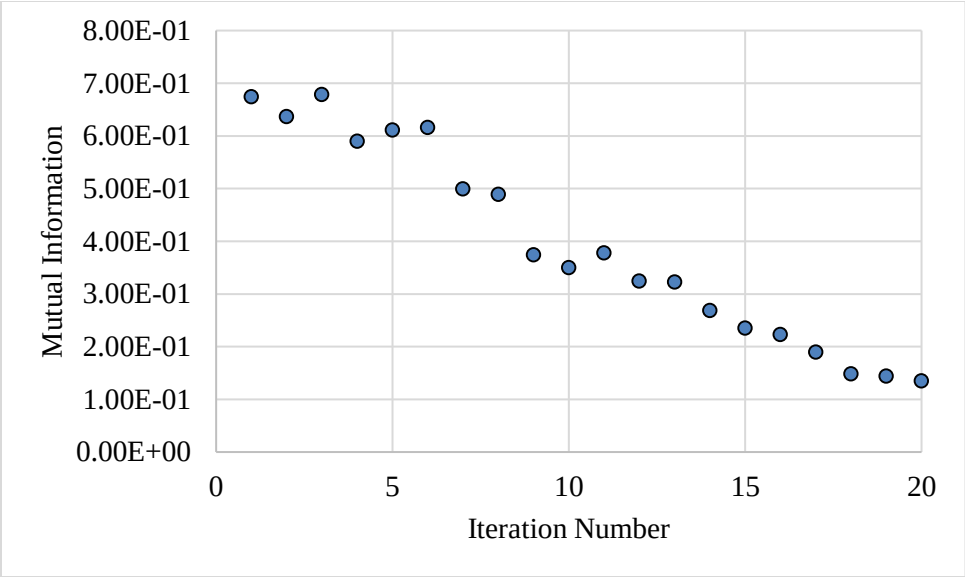

Figure 19. Plot of the mutual information for each iteration during the STAR Experimental Design process. As expected, the general trend of the mutual information is decreasing from the first iteration to the last iteration.

As an expected result of the Experimental Design process, the mutual information value generally decreased with each successive iteration. If the mutual information were consistently increasing or oscillating with successive iterations, it would be an indication that something with the Experimental Design setup or process was not functioning properly. Another way to evaluate the effectiveness of the Experimental Design process is to plot the KDE distributions of the MCMC Beta chains. This is plotted in Figure 20.

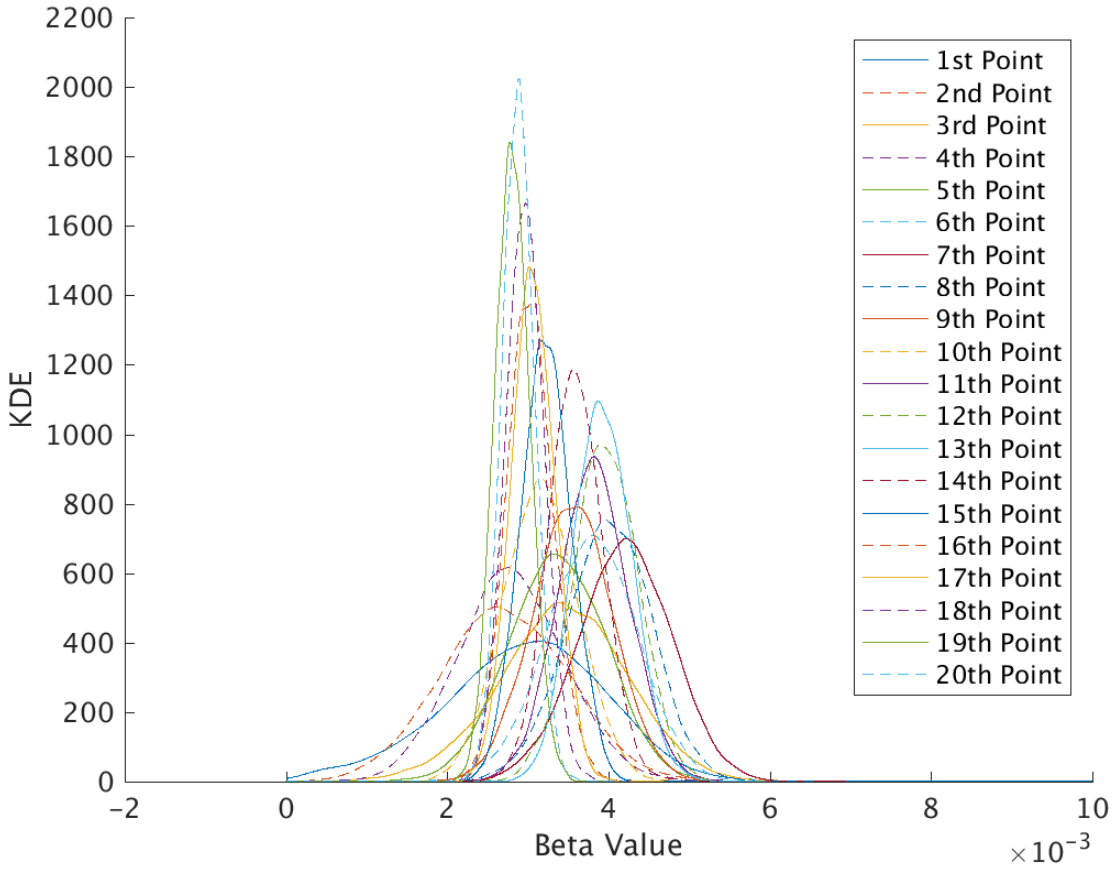

Figure 20. KDE of the MCMC results from the Bayesian Calibration performed during each STAR Experimental Design iteration. Points 2-20 added to the Experimental Design were STAR outlet temperatures while the first point was experimental data taken one of the calibration tests.

The shortest and widest peak is the experimental test that was used as the prior in Dakota. The other peaks are from each of the iterations with STAR over the experimental configurations. Ideally, the peaks would be normally distributed about a positive value of Beta and converge after several iterations to an optimal Beta value. When the experimental outlet temperatures were used as the prior, Dakota calculated 0.004050 as the median value of Beta and 0.003075 as the mean value of Beta. Note that the first distribution (1st Point in Figure 20) is not a normal distribution, therefore the median and mean differ. In this situation, Beta optimal would be based on the median value instead of the mean to mitigate the influence of skewness. When 19 iterations of STAR temperatures were introduced to Dakota, the distribution becomes approximately normally distributed, where the median and mean are equal, and yields an optimal Beta value of 0.002881.

The Experimental Design process was repeated treating the experimental data from WEC as high-fidelity results to observe differences in Beta optimal between a process using STAR and one using the experimental data. The optimal Beta value was reached 20 iterations into the process just like before and the mutual information as a function of Experimental Design iteration is given in Figure 21.

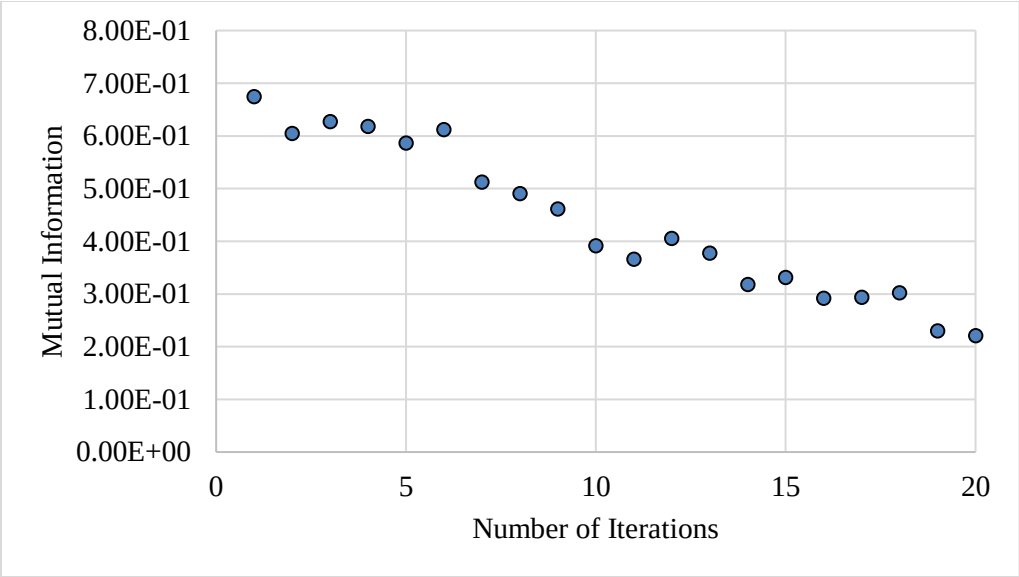

Figure 21. Plot of the mutual information for each iteration of the Experimental Design process using only experimental data. As expected, the general trend of the mutual information is decreasing from the first iteration to the last iteration.

As with the STAR Experimental Design, the mutual information generally decreases as the number of iterations increases with slight oscillations. The mutual information at iteration 1 is the same as that for the STAR Experimental design. This is expected since both Experimental Design processes began with the same prior. The minimum mutual information value at iteration 20, however, is 0.22 for the experiment only design process compared to 0.14 of the STAR design process. This implies that the STAR temperatures are providing information on Beta to the Experimental Design process more quickly than the design process using only the experimental outlet temperatures.

As with the STAR Experimental Design, the KDE distributions of the MCMC Beta chains are provided in Figure 22.

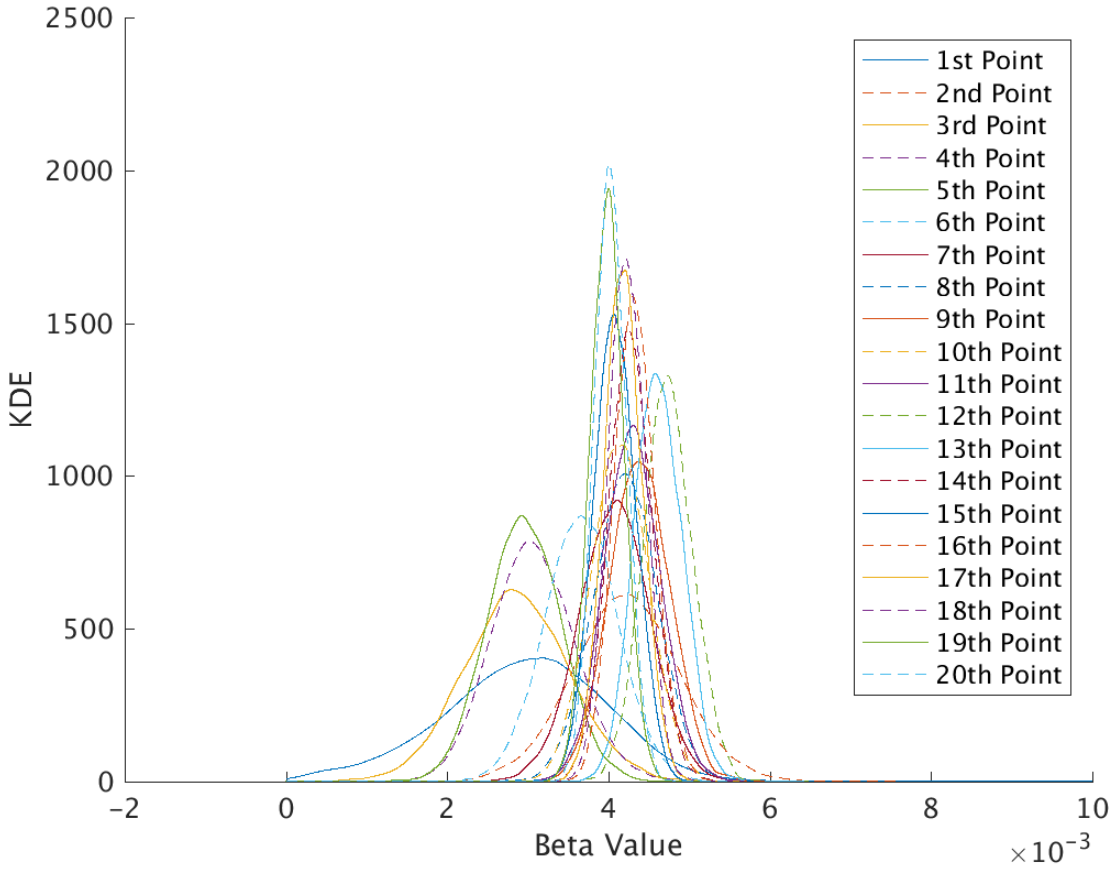

Figure 22. KDE of the MCMC results from the Bayesian Calibration performed during each Experimental Design iteration. Each of the points added to the Experimental Design were experimental outlet temperatures.

The KDEs in Figure 22 appear to converge faster than the STAR Experimental Design process. The optimal value of Beta calculated by Dakota fluctuates from iteration to iteration (where the peaks are shorter and broader), until converging on the optimal solution (where the peaks are tall and narrow). For the NMV experimental data, the optimal value of Beta calculated by Dakota was 0.004025. This value of Beta optimal is on the order of what was expected based on the WEC proposed nominal value of 0.006, but differs from the 0.002881 Beta value calculated through the STAR design process. Theories related to the inconsistency between the experimental optimal Beta value and the STAR optimal Beta value are provided in Section 8.3.

8.3 Theories on the Discrepancy Between Experiment and STAR

The process to calibrate CTF to experimental data and STAR data was demonstrated in this document. When CTF was calibrated to the experimental data, the optimal Beta value was 0.004025, however, when calibrated to STAR, the optimal value was 0.002881. It was the hope of this work that calibrating Beta to STAR results would yield a similar Beta optimal value as calibrating to the experimental data. This proved not to be the case and several theories as to why are given in the following sections.

8.3.1 Small Changes in Outlet Temperature

First, it is important to emphasize that in this application there are small changes in the outlet temperature solution as illustrated in Figure 23. Figure 23 is a comparison of two different perturbations to the experiment. The number of subchannels are given on the x-axis and the y-axis represents the outlet temperatures. There is a small amount of crossflow induced by the density dependence on temperature (note that there is no pressure dependence). The water heats up more in a "hot" subchannel than a "cold" subchannel since both have the same mass flow rate at the inlet to the assembly. A "hot" subchannel is defined as a subchannel surrounded by four higher power rods and a "cold" subchannel as a subchannel without any adjacent high power rods. Due to higher temperature, the density in a "hot" subchannel decreases. In order to move the same mass with a smaller density, the "hot" subchannel velocity must increase. This increase in velocity will cause a larger pressure drop due to friction. This subchannel pressure difference causes crossflow between the "hot" and "cold" subchannels.

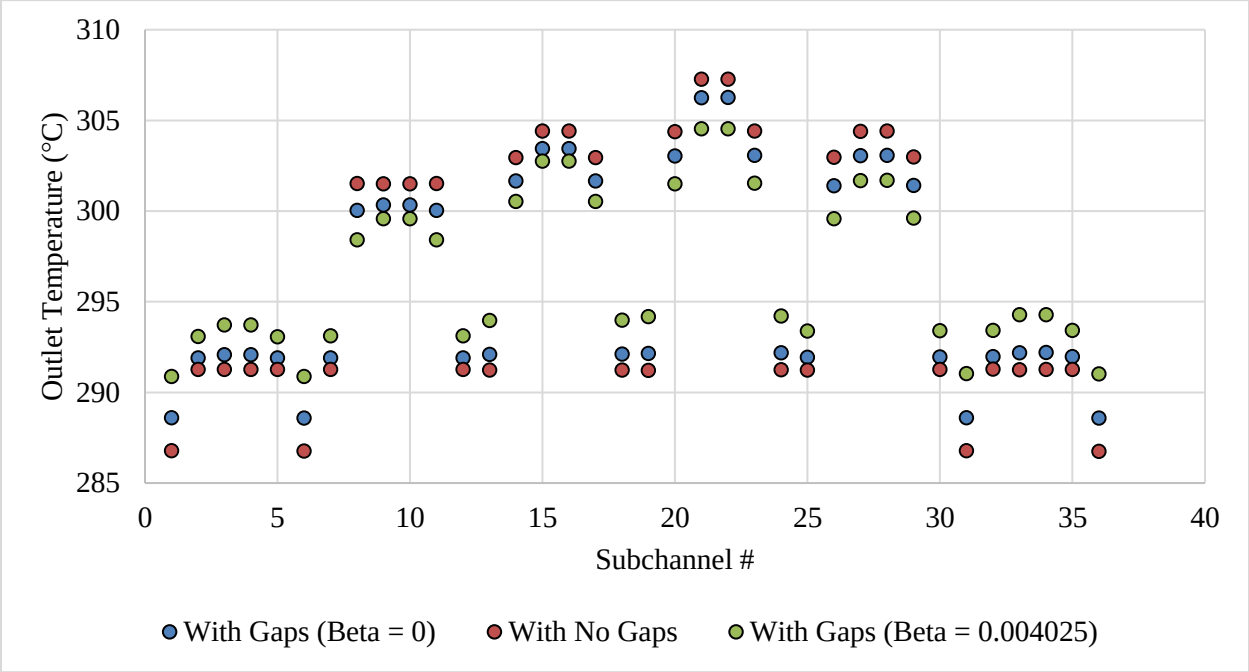

Figure 23. Comparison of the effects on outlet temperature of changing Beta versus changing crossflow in CTF.

Figure 23 provides a comparison of the change in outlet temperature due to crossflow to the change in outlet temperature due to a change in Beta. The red dots represent a CTF simulation with a Beta value of 0 and cross flow zeroed out by setting the crossflow area (the gaps between subchannels) to zero. The blue dots are the outlet temperatures from a nominal CTF simulation with Beta equal to 0 (non-zero crossflow area) and the green dots represent a CTF simulation using the optimal value for Beta, 0.004025.

It is apparent that the blue dots (Beta = 0) lie in the middle of the red dots (gap area = 0) and the green dots (Beta = 0.004025). The blue dots appear halfway between the red and green dots for the hot subchannels, but closer to the red dots in the colder subchannels. This demonstrates that the effect of calibrating Beta is similar to the change in temperature caused by crossflow and that the effect of changing Beta is larger in the cold subchannels than in the hot subchannels.

In summary, it is difficult to determine which small changes are important and which are unimportant. More detail would be needed to make a determination. The nature of the experimental data available makes it difficult to separate the effects due to the physics in the experiment and the effects of manufacturing errors and thermocouple miscalibration.

8.3.2 Differences in Symmetry

Symmetry is a factor leading to the discrepancy witnessed between STAR and the experiment in the Experimental Design step. The STAR and CTF outlet temperatures are symmetric while the experimental outlet temperatures are not symmetric. It is not apparent that the experimental results should be asymmetric. This difference in symmetry should not be confused with the level of turbulent mixing flattening the solution and causing the subchannel temperatures to shift closer to the average temperature. It is not obvious, however, that physical turbulence would result in a lack of symmetry. It is apparent that no calibration of a global Beta parameter could produce asymmetric results. Asymmetric outlet temperature could only be produced by asymmetric local values of Beta. The symmetry discrepancies are evident in Figure 24.

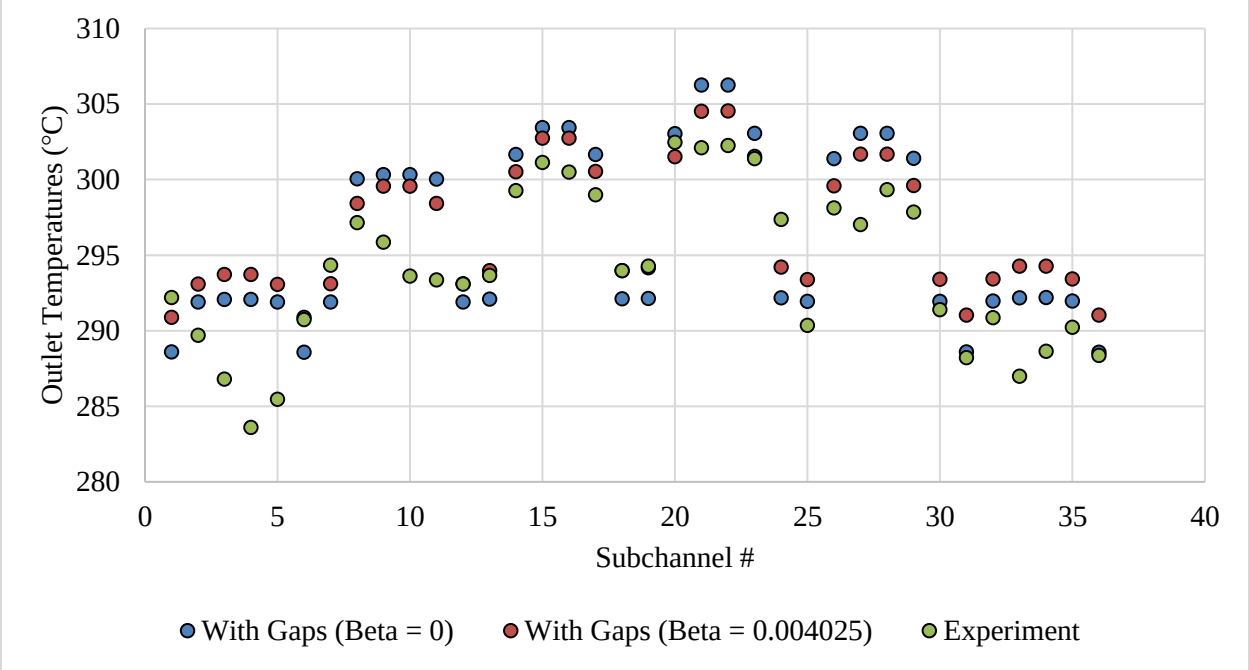

Figure 24. Graphical evidence of Beta's inability to capture the experimental asymmetry.

The blue dots in Figure 24 represent a CTF simulation with no turbulent mixing (Beta = 0) and the red dots are a result of a CTF simulation with turbulent mixing (Beta = 0.004025). Clearly the blue and red outlet temperatures display symmetry. When the experimental outlet temperatures are added (green dots), the asymmetry of the experimental data is evident. Statistically, the red dots with turbulent mixing are closer to the green dots of the experiment, but for any subchannel it is not clear that the turbulent mixing captures the unresolved physics. Some of the red dots are closer to the green dots than the blue dots and some are further away.

The question is whether the asymmetry in the experiment represents real physics and therefore some of the geometry or physics is missing in STAR, or is caused by asymmetry in the experimental geometry during manufacturing. Since the asymmetry in the experimental data is not easily captured in the STAR geometry and mesh, a method for capturing it in STAR needs to be determined.

Unphysical asymmetry could be caused by poor calibration of the thermocouples in the experiment. Poorly tuned thermocouples can convert a symmetric signal to an asymmetric result. This issue could be resolved by calibrating the thermocouples individually or in groups instead of as a lumped set.

Unphysical symmetry could also be caused by damage to the thermocouples imparted during critical heat flux (CHF) experiments performed between turbulent mixing experiments. Calibration of the thermocouples at the beginning of each test could address this issue.

8.3.3 Experimental Uncertainty Questions

Experimental uncertainty in the experimental data is another unknown for this application. The best method to measure experimental uncertainty is by conducting repeated experiments at the same experimental conditions. The set of NMV data provided for this application did not contain any repeated experimental tests. The two tests with the closest experimental conditions had the same mass flow rate and heat flux, but different inlet temperatures. These two tests are plotted together in Figure 25.

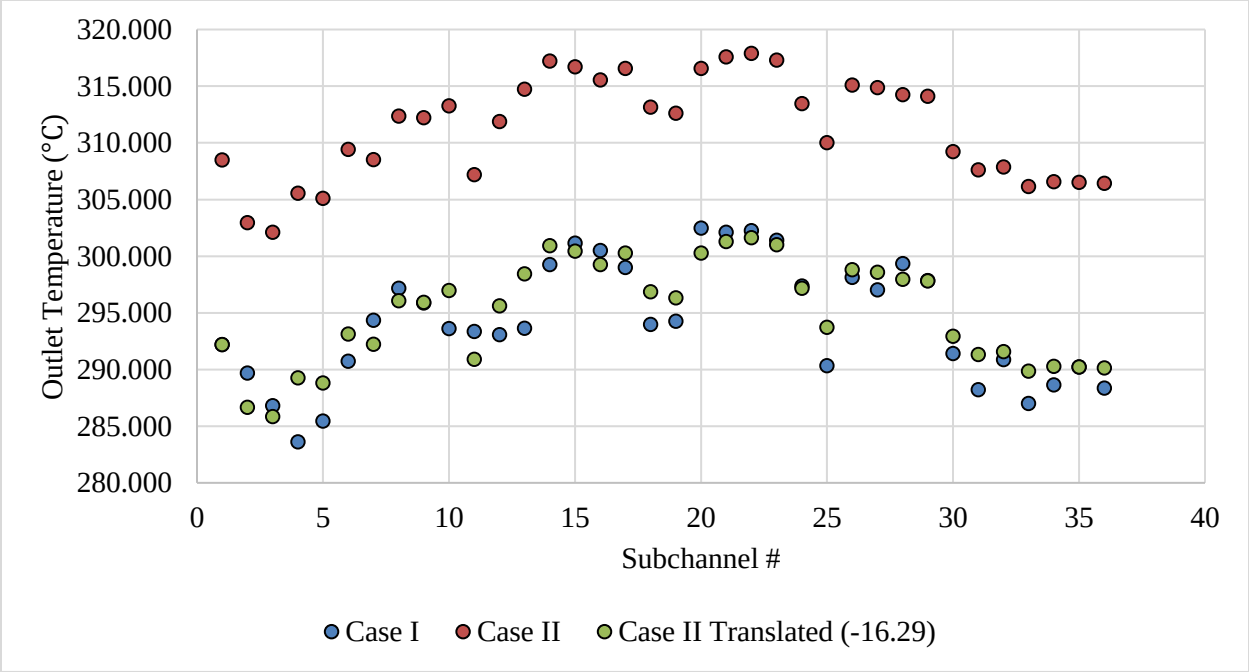

Figure 25. Pseudo experimental repeatability can be achieved when test Case I and test Case II have the same inlet mass flow rate and heat flux, but different inlet temperatures.

Figure 25 represents the closest to repeating an experiment as possible given the set of data provided. The two experiments, test Case I in blue and test Case II in red, had different inlet temperatures so the outlet temperatures from test Case II were translated down until the subchannel one temperatures aligned. The purpose of this plot is to determine if the asymmetry in the experiments is repeatable between tests. On average, the blue and green dots appear similar but the temperatures on the individual subchannels differ by as much as five degrees. Based on this figure, it is possible to infer that at least some portion of the asymmetry in the experimental outlet temperatures is a result of experimental uncertainty.

9. CTF STEP 6: 3RD QUANTITATIVE VALIDATION

A third validation step was performed to determine the improvement in CTF outlet temperatures, when compared to experimental data, as a result of the Experimental Design and Bayesian calibration performed in CTF Step 5 when 21 data sets were used to calculate Beta optimal. As noted in Section 8.2, the Experimental Design process using STAR outlet temperatures produced a different optimal Beta value than the same process using experimental outlet temperatures as the high-fidelity data. Figure 26 provides a side-by-side comparison of the last iteration from each experimental design process.

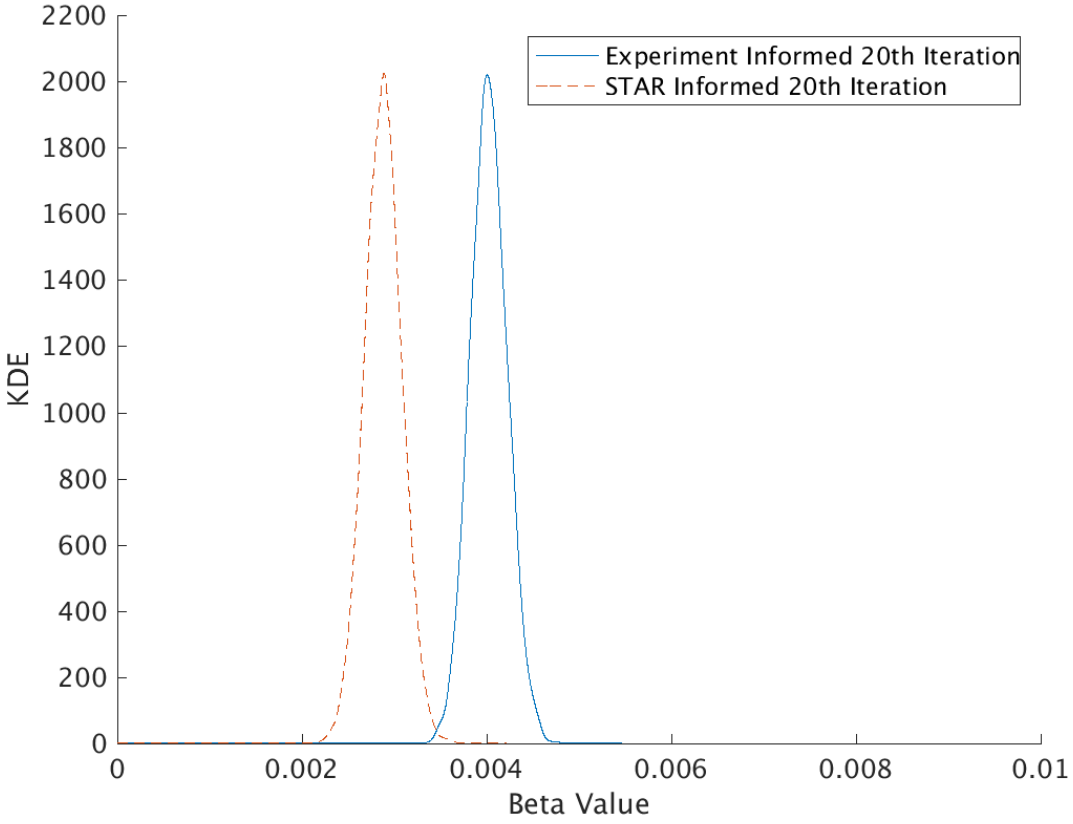

Figure 26. Graphical comparison of the KDEs produced from the final iteration of the Experimental Design process using the experimental data and STAR.

The STAR Experimental Design predicted a Beta optimal of 0.002881 whereas the design process with the experimental data predicted an optimal value of 0.004025. In Figure 26 it is evident that there is also very little overlap in the experiment and STAR KDE distributions. Section 8.3 explored possible explanations for this discrepancy, with the most obvious reason being a difference in symmetry.

Since the extent of the differences between the experimental data and STAR cannot be determined with the limited experimental data available, the final validation step was performed twice to compare the L_2 differences between the STAR-informed Beta optimal value and the experiment-informed Beta optimal value.

9.1 Experiment Informed Beta Optimal

A third validation step was performed to determine the improvement in CTF outlet temperatures due to the experiment-informed Experimental Design process and Bayesian calibration performed in Step 5 using all 21 experimental data sets. Table 9 provides a summary comparison of the individual test L_2 norms using a Beta of 0, 0.003197, and 0.004025 as well as comparing overall L_2 values from each validation step performed. A Beta value of 0 was used in the initial validation (CTF Step 1) as the starting value before using any experimental data to influence which value of Beta should be used. The Beta value from the second validation was calculated by performing a Bayesian calibration (CTF Step 3) using one of the 11 experimental calibration tests to determine the improvement made by calibrating with one experimental test. The third validation uses the Beta optimal value determined in the Experimental Design step using the experimental data sets as high-fidelity results. The selection of this Beta optimal value was influenced by all 21 of the experimental data sets to understand how much improvement can be made from using all of the available data.

Table 9. L_2 norm comparison, for each experimental test and overall, between the initial validation with a Beta value of 0, the second validation that was performed after Bayesian Calibration identified a Beta optimal value of 0.003197, and after the second Bayesian Calibration (experiment-informed) specified a Beta optimal of 0.004025.

Test Number	Initial Validation (Beta = 0)	2nd Validation (Beta = 0.003197)	3rd Validation (Beta = 0.004025)
1	0.01235	0.01144	0.01131
2	0.01351	0.01342	0.01356
3	0.01369	0.01292	0.01297
4	0.01279	0.01247	0.01261
5	0.01378	0.01318	0.01321
6	0.01093	0.01079	0.01087
7	0.01396	0.01309	0.01308
8	0.01405	0.01295	0.01292
9	0.01660	0.01596	0.01608
10	0.02223	0.01997	0.01988
Overall L_2	0.0144	0.0136	0.0136

The overall L_2 value remained approximately the same when using 21 of the experimental data points in the Experimental Design when compared to using one experimental data point in the first Bayesian calibration step. This result was not anticipated, as adding more experimental points should improve the calibration of CTF to the experiment. A graphical representation of Table 9 is given in Figure 27.

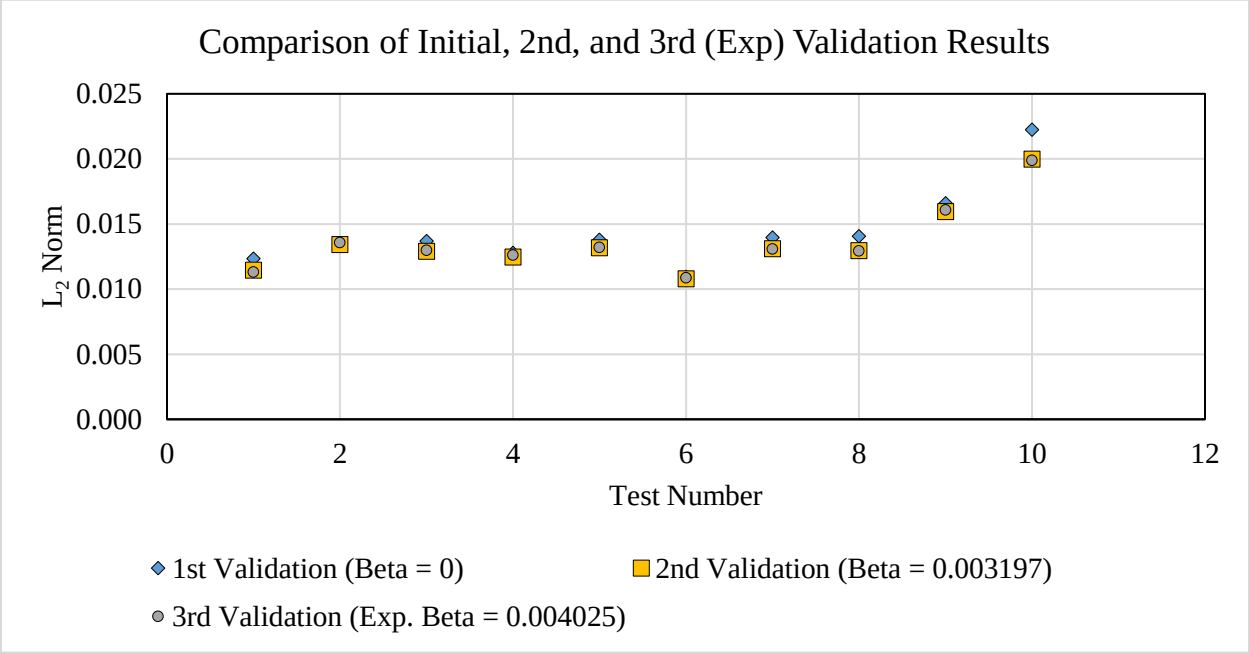

Figure 27. Graphical comparison of the L_2 values from the initial validation compared to the L_2 values from the second and final validations.

Not much improvement was made through the Experimental Design process for this application. The lack of progress is due in part to the fact that statistically, CTF outlet temperatures were approximately 1.4% different from the experiment outlet temperatures before the first calibration was performed and significant improvement is not likely. The biggest reason, however, for not observing more improvement is the differences in symmetry between CTF outlet temperatures and the experimental outlet temperatures. CTF is perfectly symmetrical and the experiment is not. Beta can only be tuned so much in this application before experiencing tuning limitations.

The expectation was that an Experimental Design process using more of the experimental data or STAR would further align the CTF outlet temperatures with the experimental outlet temperatures, however, this was not the case. As evident in Figure 28, the experimental outlet temperatures exhibited a shape not shared by the simulation. Improvement was made during the first Bayesian calibration of Beta using one experimental test, but the Experimental Design could not further reduce the discrepancy between CTF and the experimental data when looking solely at the distance between the experimental data and CTF (L_2 norms).

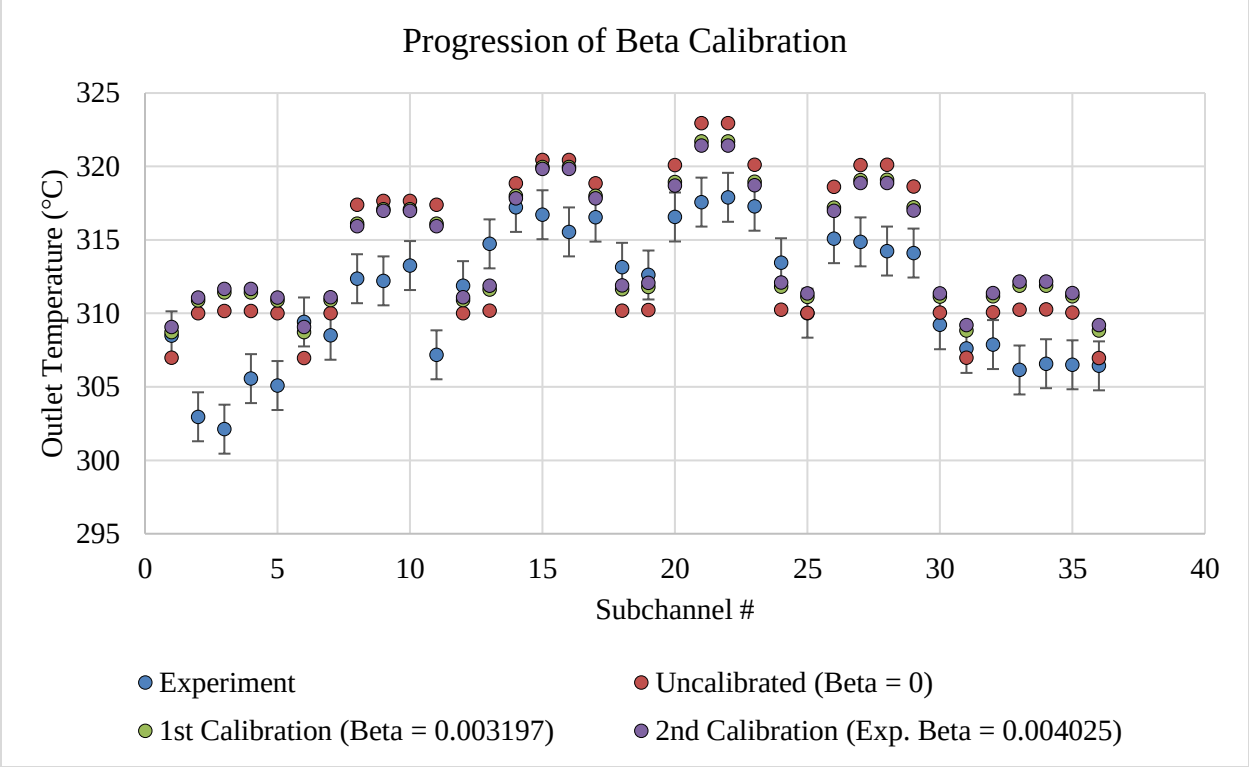

Figure 28. Comparison of the experimental outlet temperatures, uncalibrated outlet temperatures, once-calibrated outlet temperatures, and twice-calibrated outlet temperatures for test Case I.

In the hotter subchannels, the twice-calibrated results appear closer to the experimental data, but at cooler subchannels, the uncalibrated results are closer. The discrepancies in the symmetry of the outlet temperatures between the simulations, both CTF and STAR, and the experiment was a major reason for the lack of significant improvement of the L_2 norms during the Hi2Lo process. While the L_2 norm does not necessarily reflect improvement in the value of Beta, Figure 22 demonstrates a reduction in the uncertainty of the optimal Beta value with the addition of successive experimental data sets, leading to higher confidence in the predicted value of Beta. The process was demonstrated; however, to truly understand the potential of Hi2Lo, a better application or more detailed set of experimental data is needed where there are not symmetry differences between the codes and the experimental data.

9.2 STAR Informed Beta Optimal

The final validation step was repeated with the optimal Beta value from the STAR-informed Experimental Design process. Table 10 provides a similar comparison as Table 9, except the Beta value used to generate the results in the third column was the result of the design process with STAR instead of the experimental data.

Column 1 presents the L_2 norm results from the initial validation step (CTF Step 1), for each validation test as well as overall, with a Beta value of 0. As a reminder, a value of 0 was chosen as the initial Beta value before using experimental data in the calibration steps to infer a more appropriate value. The L_2 norm results in column 2 were calculated during the second validation step based on the optimal Beta from the Bayesian calibration step (CTF Step 3). The optimal Beta value used in the second validation was determined by using 1 of the 11 experimental calibration tests to calibrate Beta. The results from the third validation, column 3, use the Beta optimal value determined from the STAR Experimental Design process. The selection of this Beta optimal value

was influenced by the outlet temperatures of 1 experimental test and 20 of the STAR validation tests to understand the improvement made when using 21 sets of data to inform the Experimental Design process.

Table 10. L_2 norm comparison, for each experimental test and overall, between the initial validation with a Beta value of 0, the second validation that was performed after Bayesian Calibration identified a Beta optimal value of 0.003197, and after the second Bayesian Calibration (STAR informed) specified a Beta optimal of 0.002881.

Test Number	Initial Validation (Beta = 0)	2nd Validation (Beta = 0.003197)	3rd Validation (Beta = 0.002881)
1	0.01235	0.01144	0.01148
2	0.01351	0.01342	0.01338
3	0.01369	0.01292	0.01291
4	0.01279	0.01247	0.01243
5	0.01378	0.01318	0.01318
6	0.01093	0.01079	0.01077
7	0.01396	0.01309	0.01311
8	0.01405	0.01295	0.01298
9	0.01660	0.01596	0.01593
10	0.02223	0.01997	0.02004
Overall L_2	0.0144	0.0136	0.0136

As with the experimental data informed Beta optimal value in Table 9, the overall L_2 value remained approximately the same when 21 sets of outlet temperatures were used instead of a single set of outlet temperatures. As stated previously, the expectation was that the L_2 norm would be lower when more data was used to inform the value of Beta optimal. A graphical representation of Table 10 is given in Figure 29.

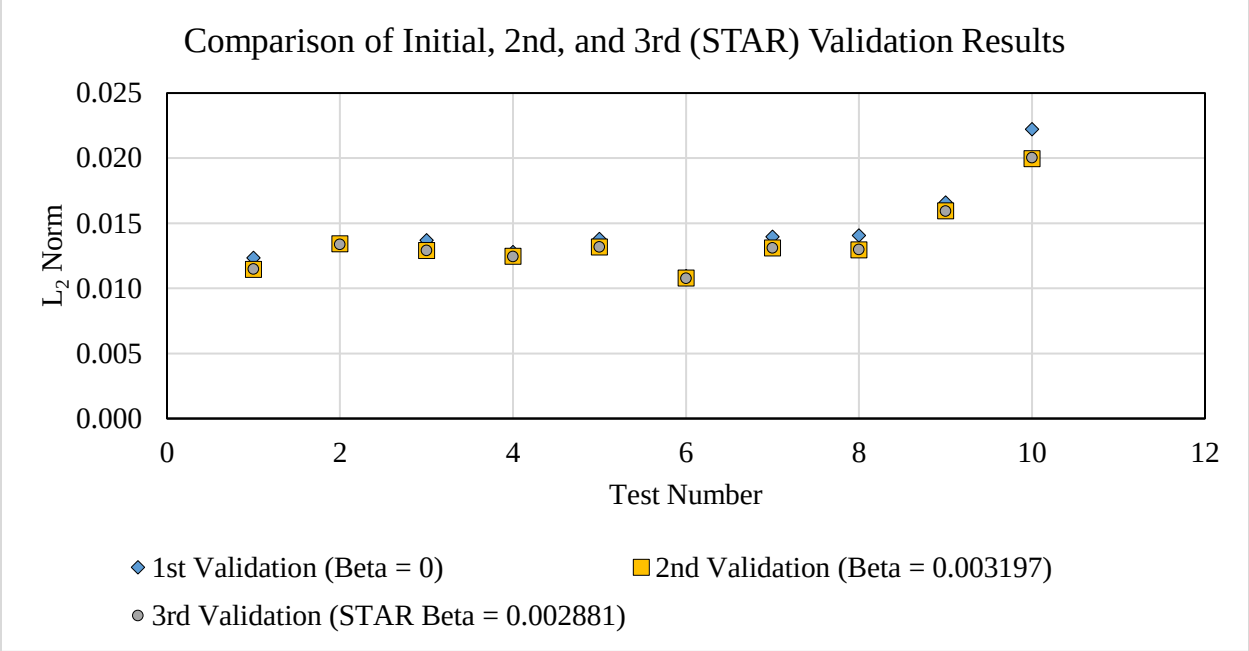

Figure 29. Graphical comparison of the L_2 values from the initial validation compared to the L_2 values from the second and final validations.

Again, not much improvement to the L_2 norm was made through the STAR Experimental Design process for this application. The expectation was that using STAR outlet temperatures instead of experimental outlet temperatures would result in lower L_2 norm values, however, the differences in outlet temperature symmetry between STAR and the experiment did not promote improvements in the fit of the CTF outlet temperatures when compared to the experiments. Beta was tuned to the STAR data, which is more similar in symmetry to CTF. This led to differences in the predicted value of Beta optimal between the STAR Experimental Design and the Experimental Design using the experimental data.

In Figure 30, the experimental outlet temperatures exhibited a shape not shared by CTF or STAR. The CTF outlet temperatures (shown in circles) follow the same symmetry as the STAR outlet temperatures (orange triangles) which differ from the experiment (blue squares).

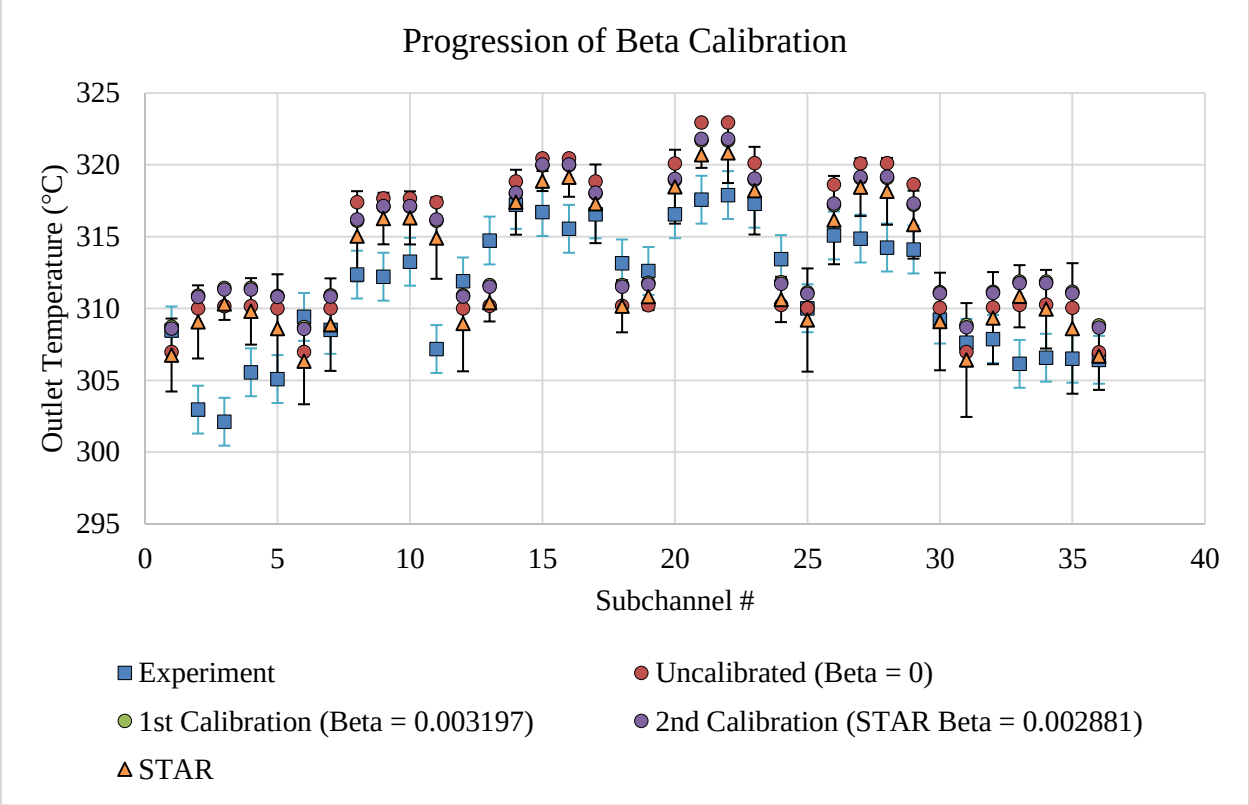

Figure 30. Comparison of the experimental outlet temperatures, uncalibrated outlet temperatures, once-calibrated outlet temperatures, twice-calibrated outlet temperatures for test Case I, and STAR outlet temperatures.

In the hotter subchannels, the twice-calibrated results appear closer to the experimental data and STAR data, but at cooler subchannels, the uncalibrated results are closer. The discrepancies in the symmetry of the outlet temperatures between the simulations, both CTF and STAR, and the experiment was a major cause for the lack of significant improvement of the L_2 norms during the Hi2Lo process. While the L_2 norm does not necessarily reflect improvement in the value of Beta through the Hi2Lo process, Figure 20 demonstrates a reduction in the uncertainty of the optimal Beta value with the addition of successive data sets, leading to higher confidence in the predicted value of Beta.

To demonstrate the consequences of differences in symmetry when calculating L_2 norms, the norms were re-calculated for the third validation step, comparing the CTF outlet temperatures using STAR-informed and experiment-informed Beta values to STAR outlet temperatures instead of the experimental outlet temperatures. The results of this comparison are provided in Table 11.

Table 11. L_2 norms comparing CTF outlet temperatures to each STAR data set after the second STAR-informed and experiment-informed Bayesian Calibrations specified a Beta optimal of 0.002881 and 0.004025 respectively.

Test Number	3rd Validation (STAR Beta = 0.002881)	3rd Validation (EXP Beta = 0.004025)
1	0.00595	0.00600
2	0.00517	0.00576
3	0.00600	0.00667
4	0.00595	0.00660
5	0.00469	0.00527
6	0.00492	0.00524
7	0.00496	0.00558
8	0.00605	0.00673
9	0.00763	0.00838
10	0.01077	0.01182
Overall L_2	0.006	0.007

When the CTF outlet temperatures from the STAR-informed Beta value are compared to the STAR data, the overall L_2 norm is reduced by 77.6% when compared to the experiment-informed CTF outlet temperature verses experimental data (third column of Table 10). Additionally, there is a 15.4% difference in the overall L_2 norm between the CTF outlet temperatures using the STAR-informed Beta value and experiment-informed Beta value when compared to the STAR outlet temperature data (Table 11). While this does not prove that the discrepancies between the experimental and STAR data are solely due to symmetry, the differences in symmetry significantly impact the calibration process.

These results indicate that the Hi2Lo process works, but, not with the set of experimental data used in this analysis. The process was demonstrated; however, to truly understand the potential of Hi2Lo, a better application or more detailed set of experimental data is needed where there are not symmetry differences between the codes and the experimental data.

While the Experimental Design process increased the confidence in the Beta optimal values calculated using the experimental data and STAR data, the two data sets did not produce a similar Beta optimal value. The lack of symmetry in the experimental data is posited as a key contributor to this discrepancy, however future work with another experimental data set or application could confirm this theory. Additionally, CTF may not be as sensitive to Beta changes as previously

believed since the L_2 norms were identical to three decimal places when the STAR-informed and experiment-informed Beta values were used to compare CTF outlet temperatures to the experimental data.

10. CONCLUSION

The work performed in this milestone outlined the steps of the Hi2Lo process. Due to questions regarding the experimental data and STAR, the final results of the analysis, when compared to experimental data, were not as anticipated, however the goal of demonstrating every step in the process and reducing the uncertainty in the selected value of Beta was achieved. While the experimental L_2 norm was not significantly improved by adding 20 additional data points through the Experimental Design process, the uncertainty in Beta optimal was reduced leading to higher confidence in a value of Beta optimal. The STAR L_2 norm was improved by adding 20 data points through the Experimental Design process. Differences in outlet temperature symmetry between the codes and the experimental data led to discrepancies in the value of Beta optimal obtained through an experiment-informed and a STAR-informed Experimental Design process, as well as reducing the improvement made when calculating L_2 norms with respect to the experimental data.

The work performed has demonstrated that it is possible to calibrate Beta to better align CTF outlet temperatures with the experimental outlet temperatures. Although it is clear that this work improved the fit of CTF outlet temperatures to the experimental data statistically, it is not obvious that adjusting the turbulent mixing parameter in CTF is capturing some unresolved physics.

The ability to calibrate Beta in CTF to STAR results was also effectively established. Both the STAR outlet temperatures and the CTF outlet temperatures (with and without mixing) are symmetric and the L_2 norm with respect to the STAR data significantly decreases through the Experimental Design process.

In terms of future work, applying the Hi2Lo framework to a problem exhibiting greater sensitivity to at least one of the calibration parameters would be more useful for demonstrating the potential of the process. This implementation of the Hi2Lo process also exposed the reality that high (and low)-fidelity calculations are often conducted under ideal conditions not often present in physical experiments, potentially leading to statistically significant differences in calibration results between simulations and experiments.

Future work should also be performed to address the symmetry in the code results and the asymmetry in the experimental results. A solution verification also needs to be performed to determine if the error due to the coarseness of the mesh is the culprit in removing the asymmetry from the STAR results. Finally, an investigation into finding a way to change the geometry or physics in the STAR simulation to enable better agreement with the experimental outlet temperatures needs to occur.

REFERENCES

1. L. N. Gilkey. *STAR-CCM+ (CFD) Calculations and Validation L3:VVI.H2LP15.02*., CASL-U-2017-1421-000, September 2017.
2. M. N. Avramova, T. S. Blyth, R. K. Salko. *CTF User's Manual*. The Pennsylvania State University. October 6, 2016.
3. B. ADAMS, L. BAUMAN, W. BOHNHOFF, K. DALBEY, M. EBEIDA, J. EDDY, M. ELDRED, P. HOUGH, K. HU, J. JAKEMAN, J. STEPHENS, L. SWILER, D. VIGIL, and T. WILDEY, *Dakota, A Multilevel Parallel Object–Oriented Framework for Design Optimization, Parameter Estimation, Uncertainty Quantification, and Sensitivity Analysis:*

Version 6.0 User's Manual, Sandia Technical Report SAND2014–4633 (July 2014), updated May 2017 (Version 6.6).
4. *Description of Non-Mixing Vane Grid CHF Test for CASL DNB Challenge Problem*, PFT-13-8, February 2013.
5. *Supplemental Information to PFT-13-8 Rev. 0 for CASL*, PFT-16-77, August 2016.
6. *Transmittal of 5x5 Non-Mixing Vane Grid Rod Bundle CFD Mesh Model to CASL*, MT-16-75, August 2016.